

LOW PRESSURE GLOW DISCHARGE PLASMA DIAGNOSTICS

by
Gülayşe Gürsoy

Submitted to the Institute of Graduate Studies in
Science and Engineering in partial fulfillment of
the requirements for the degree of
Master of Science
in
Physics

Yeditepe University

2012

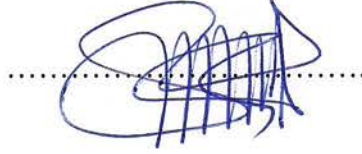
LOW PRESSURE GLOW DISCHARGE PLASMA DIAGNOSTICS

APPROVED BY:

Prof. Dr. Necdet Aslan
(Supervisor)



Prof. Dr. Şahin Aktaş



Assoc. Prof. Dr. Sinan Keskin



Assist. Prof. Dr. Ercüment Akat



DATE OF APPROVAL: / /

ACKNOWLEDGEMENTS

This thesis arose in mainly of the results of the experiments that have been conducted at Vacuum and Plasma Laboratory of Yeditepe University since it was established.

I have been partially supported by The Scientific and Technological Research Council of Turkey (TUBITAK) under grant 110T578 during my thesis work.

Foremost, I would like to express my sincere gratitude to my advisor Prof. Dr. Necdet Aslan for his continuous support and guidance throughout my MSc study. With his encouragement, his enthusiasm, his inspiration, his immense knowledge and his great efforts to explain things clearly and simply, he made this thesis possible.

Besides my supervisor, I would like to thank my friend and colleague Turgay Çoruhlu for his inexhaustible patience and his kind assistance with reading the manuscript, giving wise advices, helping with various applications, and so on. I would have been lost without him.

Finally, I wish to thank my family. They have always supported me. To them I dedicate this thesis.

ABSTRACT

LOW PRESSURE GLOW DISCHARGE PLASMA DIAGNOSTICS

In this thesis, the breakdown voltage, plasma potential for air and argon glow discharges and light emission spectroscopy for argon discharge are investigated. A DC high voltage supply was designed to do the experiments. By conducting experiments, firstly, Paschen voltages measurements for air and argon are shown. Secondly, by using the double probes the plasma potential measurements for air and argon are performed. There is a good agreement with the literature results. Finally, the emission spectrum of the argon plasma, taken by Baki spectrometer, is examined. Using the locations of the peaks, the ions generated in the argon discharge are found.

ÖZET

DÜŞÜK BASINÇ PARLAK DEŞARJIN PLAZMA DİAGNOSTİĞİ

Tezde hava ve argon parlak (akkor) deşarj plazmalarının sınır gerilimi, plazma potansiyeli ve argon parlak deşarj plazmasının ışık emisyon spektroskopisi incelenmektedir. Deneyleerde kullanılmak üzere yüksek DC gerilim kaynağı tasarlanmıştır. Yürütölen deneyleerle, ilk olarak hava ve argonun Paschen gerilimi ölçümleri gösterilmiştir. Sonra, çift prob kullanılarak hava ve argon için plazma potansiyeli ölçümleri yapılmıştır. Deneyle sonuçları literatürdeki referans sonuçlarla uyumludur. Son olarak, Baki spektrometre kullanılarak elde edilen argon plazmasının ışık emisyon tayfı incelenmiştir ve tepe noktalarının yeri yardımıyla argon plazmasında oluşun iyonlar bulunmuştur.

TABLE OF CONTENTS

ACKNOWLEDGEMENTS.....	iii
ABSTRACT.....	iv
ÖZET.....	v
TABLE OF CONTENT.....	vi
LIST OF FIGURE.....	viii
LIST OF TABLE	xiii
1. INTRODUCTION.....	1
2. DC GLOW DISCHARGES	4
2.1. Architecture of the Discharge.....	4
2.2. Maintenance of the Discharge	8
2.3. Secondary Electron Emission.....	9
2.3.1. Electron Bombardment.....	10
2.3.2. Ion Bombardment.....	11
2.3.3. Neutral Bombardment	16
2.3.4. Photon Bombardment.....	17
2.4. The Cathode Region.....	18
2.4.1. Ionization in the Sheath.....	20
2.4.2. Structure of the Cathode Sheath	22
2.4.3. Application to Glow Discharge Sheaths.....	24
2.5. The Anode Region	26
3. PLASMA POTENTIAL	28
3.1. Sheath Formation at a Floating Substrate	30
3.2. Probe Characteristics.....	35
3.2.1. Practical Complications.....	38
3.2.2. Positively Biased Probes	39
3.3. Sheath Formation and Bohm Criterion	41
4. THE ELECTRICAL PROBE METHOD	47
4.1. A Two-Electrode System	47
4.2. The Double Probe System.....	51

4.3. The Single Probe System	52
4.4. Elementary Probe Theory for Low Pressure Plasmas.....	55
4.4.1. Elementary Treatment of Positive Ion Collection.....	57
4.4.2. Elementary Treatment of Electron Collection	60
4.4.3. Simple Determination of Plasma Parameters	61
5. EXPERIMENTAL RESULTS.....	63
5.1. Breakdown Voltage and Paschen Curve	68
5.2. Probe Measurements	73
5.3. Plasma Diagnostics	80
6. CONCLUSION	83
7. REFERENCES.....	84

LIST OF FIGURES

Figure 1.1.	Energy transfer from the field to the electrons and ions.....	2
Figure 2.1.	$I - V$ characteristic for Cr sputtering in argon.....	5
Figure 2.2.	The normal glow discharge in neon in a $50cm$ tube at $p = 1 torr$	6
Figure 2.3.	DC glow discharge process.....	6
Figure 2.4.	Voltage distribution in a DC glow discharge process.....	8
Figure 2.5.	The energy distribution of secondary electrons emitted by Ag , a. elastically reflected primaries, b. inelastically reflected primaries, c. 'true' secondaries.....	10
Figure 2.6.	Secondary electron coefficient γ_i of different metals as a function of the energy of incident electrons [11].....	11
Figure 2.7.	Secondary electron yields γ_i for noble gas ions on atomically clean W and Mo [12].....	12
Figure 2.8.	Secondary electron coefficient γ_i for ions of energy K falling on the surface of various substances [8].....	13
Figure 2.9.	Variation of γ_i with ion energy for Ar^+ bombardment of (1 1 1) (1 0 0) and (1 1 0) surfaces of a. Ni , b. Al , c. Ag and d. Mo [8].....	14

Figure 2.10.	Secondary electron yields γ_i for He^+ and Ne^+ ions, as a monolayer of N forms on W . The break in the plot represents the completion of the first monolayer [13].....	15
Figure 2.11.	Secondary coefficient γ_i for Ar ions on clean W and W covered with a monolayer of N [13].....	15
Figure 2.12.	Secondary electron emission as a function of energy for Ar ion and neutral atom bombardment of Mo [14]	16
Figure 2.13.	Photoelectric yield γ_p as a function of the wavelength λ of the incident light (energy E of quantum) for various substances [8].....	18
Figure 2.14.	Discharge loss processes.....	19
Figure 2.15.	Ion pair production in the dark space	20
Figure 2.16.	Analysis of ion pair production in the dark space.....	21
Figure 2.17.	Regions of a cathode sheath.....	23
Figure 2.18.	Electron energy diagram for the DC glow discharge	23
Figure 3.1.	Negative, positive and neutral atoms.....	29
Figure 3.2.	Initial particle fluxes at the substrate.....	30
Figure 3.3.	Variation of electrical potential (upper) and of the potential energies of electrons and positive ions (lower) in the vicinity of an electrically floating substrate	31

Figure 3.4.	A space charge sheath develops in front of a floating substrate (upper), and establishes a sheath voltage (lower).....	33
Figure 3.5.	Schematic representation for measurements in a plasma	35
Figure 3.6.	Current density-voltage characteristics of a probe	36
Figure 3.7.	Typical probe characteristics showing a quasi-linear region where $\log j \propto (V - V_s)$ [22]. Tantalum target 1000cm^2 . Argon discharge at 10 mTorr , 3 keV and 59 mA	37
Figure 3.8.	Effective current-collecting areas of probes	39
Figure 3.9.	Schematic of probe and discharge circuits.....	40
Figure 3.10.	Potential variation near a negative electrode. Density $n_i(x)$ and potential $V(x)$ at $x \geq 0$	42
Figure 3.11.	Variation of ion and electron density with potential $V(x)$ in a sheath for $U_0 > (kT_e/m_i)$ and $U_0 < (kT_e/m_i)$	45
Figure 4.1.	Two-electrode circuit.....	48
Figure 4.2.	Potential distribution in a two-electrode system	49
Figure 4.3.	Typical double-probe characteristics.....	52
Figure 4.4.	Single probe circuit.....	54
Figure 4.5.	Single probe characteristics	54
Figure 4.6.	Potential distribution in the vicinity of a negative probe.....	58

Figure 4.7.	Graph of $\ln I_s $ versus V_a for deducing the electron temperature.....	61
Figure 4.8.	Correction for the positive ion contribution to the probe current	62
Figure 5.1.	Experimental setup	64
Figure 5.2.	The design of <i>DC</i> power supply ($R = 1k\Omega$, a capacitor bank with $C_{eq} = 2\mu F$, a diode, and transformer)	64
Figure 5.3.	Glow discharge.....	65
Figure 5.4.	Probe measurements	65
Figure 5.5.	The view of the glow discharge probe measurements at the outside of the chamber	66
Figure 5.6.	Glow discharge occurred around the cathode	66
Figure 5.7.	Inside of the vacuum chamber with probes	67
Figure 5.8.	There are 19 probes and the measurements are taken between the subsequent two probes.....	67
Figure 5.9.	The change in pressure with time.....	68
Figure 5.10.	Voltage vs Pd for air	71
Figure 5.11.	Voltage vs Pd for Argon.....	72
Figure 5.12.	Double probe measurements from the oscilloscope for air at the pressure of 40 and 60 <i>mTorr</i>	74

Figure 5.13. Double probe measurements from the multimeter for air at the pressure of 45.5 mTorr	74
Figure 5.14. Double probe measurements when there is partial $\approx 1/4$ Ar at the pressure of 116 mTorr	78
Figure 5.15. Double probe measurements when there is mostly ($\approx 3/4$) Argon (Ar) at the pressure of 114 and 142 mTorr	80
Figure 5.16. Background measurement of wavelength versus intensity at 30 mTorr	81
Figure 5.17. Wavelength versus intensity at high pressure of 90 mTorr	81
Figure 5.18. Background measurement of wavelength versus intensity at high pressure of 150 mTorr	82

LIST OF TABLES

Table 3.1.	Typical parameter values for a glow discharge plasma.....	29
Table 5.1.	The values of pressure \times separation distance and voltages for air	70
Table 5.2.	The values of pressure \times separation distance and voltages for Argon..	71
Table 5.3.	Double probe measurements from the oscilloscope for air at the pressure of 40 and 60 <i>mTorr</i>	73
Table 5.4.	Double probe measurements from the multimeter for air at the pressure of 45.5 <i>mTorr</i>	75
Table 5.5.	Double probe measurements when there is partial $\approx 1/4$ Ar at the pressure of 116 <i>mTorr</i>	77
Table 5.6.	Double probe measurements when there is mostly ($\approx 3/4$) Argon (Ar) at the pressure of 114 and 142 <i>mTorr</i>	79
Table 5.7.	According to the locations of the peaks, the ions generated in the discharge	82

1. INTRODUCTION

Any ionized gas cannot be called a plasma, because there is always some small degree of ionization in any gas. A plasma is a quasi-neutral (significantly ionized) gas of charged and neutral particles which exhibits collective behaviour and obeys Maxwell-Boltzmann statistics [1-5].

In the type of plasmas we considered, the degree of ionization is typically only 10^{-4} , so the gas consists mostly of neutrals. Although the Coulomb interaction between the charges is both strong and long-range, it is possible to assume for an undisturbed plasma that the charges move around as free particles, since the sum of all the interactions tends to cancel. However, there are situations where the Coulomb interaction becomes dominant, as for example when the plasma is perturbed.

Assume that the charged particles are singly charged positive ions and electrons. Moreover, descriptions of the plasma will be made in the context of the glow discharge processes being considered. The essential mechanisms in the plasma are excitation and relaxation, ionization and recombination. To maintain a steady state of electron and ion densities, the recombination process must be balanced by an ionization process, i.e., an external energy source is required. In practice, that energy source is an electric field, which can act directly on the charged particles only. Let m_i and m_e be the masses of the ion and electron respectively. Consider an electric field E acting on an initially stationary ion. The work done by the electric field and hence the energy transferred to the ion, will be Eex where x is the distance travelled in time t . Moreover,

$$x = \frac{1}{2}at^2 \quad (1.1)$$

where a is the acceleration due to the field in Figure 1.1. Then

$$Ee = m_i a \quad (1.2)$$

hence, the work done is

$$W = Eex = Ee \frac{1}{2} \frac{Ee}{m_i} t^2 = \frac{(Eet)^2}{2m_i} \quad (1.3)$$

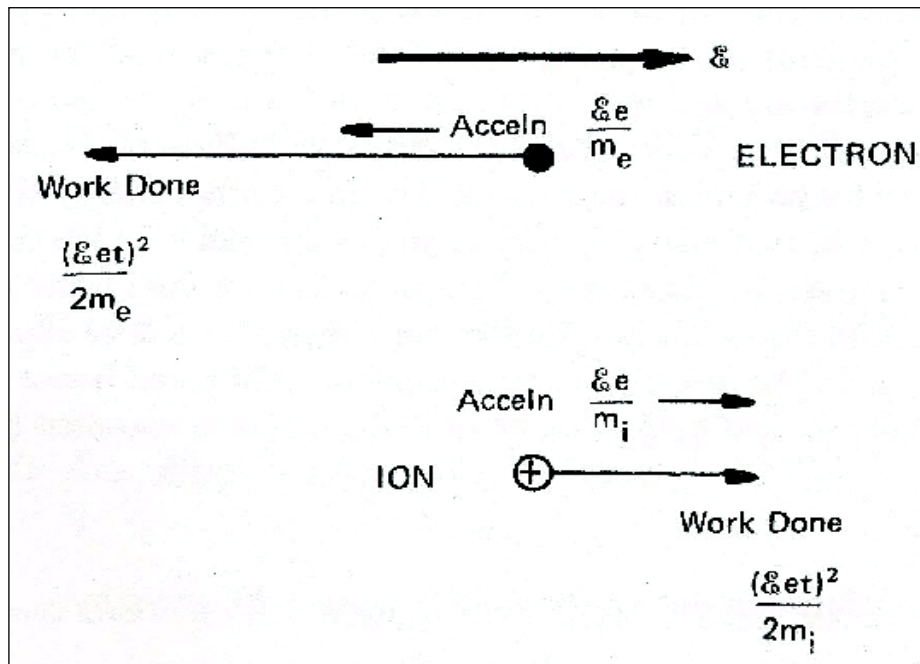


Figure 1.1. Energy transfer from the field to the electrons and ions. The figure is taken from Chapman, B.N., Glow Discharge Processes [2]

A similar relationship holds for the electrons, but since $m_i \gg m_e$, the action of the field is primarily to give energy to the electrons. The argument above ignored collisions and we can always choose t to be short enough that this is so. However, we have seen that, in general, collisions abound in plasmas. Electrons collide with neutral atoms and ions, but only a very small energy transfer to the heavy particles can take place. In turn, the neutral atoms and ions share their energy efficiently in collision processes and likewise lose energy to the walls of the chamber. The net result is that electrons can have a high average kinetic energy, which might typically be 2 – 8 eV. The ions, which can absorb just a little energy directly from the electric field, have an average energy not much higher than that of the neutral molecules, which gain energy above the ambient only by collisions with ions (effectively) and electrons (ineffectively) and remain essentially at room temperature. We know that for the neutral gas atoms

$$\frac{1}{2}m\overline{v^2} = \frac{3}{2}kT \quad (1.3)$$

The average energy is characterized by the kT term and although this would conventionally be measured in *ergs*, it is more convenient here to work in electron volts. It is useful to remember that kT has a value of $1/40 \text{ eV}$ at 290 V , i.e. about room temperature.

The concept of temperature applies to a random, i.e. Maxwell-Boltzmann, distribution. Based on an expectation of a large number of electron-electron collisions and other interactions and very efficient energy sharing amongst the electrons because the energy transfer function takes all values between 0 and 1 for equal mass particles as the impact angle θ , varies, a Maxwell-Boltzmann distribution seems quite reasonable. Since

$$\frac{1}{2}m_e\overline{v^2} = \frac{3}{2}kT_e \quad (1.4)$$

applies to electrons, too, we can associate an effective temperature T_e with the electron motion. Measurements on glow discharge plasmas yield average electron energies around 2 eV , which corresponds to an electron temperature of 23200 K . That does not mean that the containing vessel will melt, and that is because the heat capacity of the electrons is too small; we just have to think more carefully about the temperature concept. Since the ions are able receive some energy from the external electric field, their temperature is somewhat above ambient, 500 K is representative.

2. DC GLOW DISCHARGES

Until now we have been dealing with rather idealized homogeneous plasma with a well-defined potential and density and with constituent particles in equilibrium motion characterized by relevant temperatures. The glow discharges which we are using only approximate this condition, for various reasons. Nevertheless, many of the plasma concepts are of great utility in helping us to derive some understanding and control of glow discharge processes, even on a semi-quantitative basis. Amongst sputtering and plasma etching folks, the words 'plasma' and 'glow discharge' tend to be used synonymously- to the horror of plasma physicists. One can get into semantic discussions and argue that some discharges are plasmas with two or three different groups of electrons each with a well-defined temperature. That argument could probably be extended indefinitely. So let us accept that our glow discharges are certainly not ideal plasmas and keep this in mind when we lapse into glow discharge-plasma synonyms.

One of the complicating factors in trying to understand glow discharges is that most of the literature, particularly the 'classical' literature of the 1920's and 30's, deals with *DC* discharges; whereas practical plasma processes are more usually *RF* excited. Also, as we said above, none of our practical glow discharges are truly plasmas. This gives then, in a sense, a choice: we can either pursue some plasma physics rather exactly and then find that it does not entirely apply to our systems; or we can follow some simpler, if not always entirely accurate, models which convey the physical ideas rather well and in the event, are probably just as accurate.

2.1. ARCHITECTURE OF THE DISCHARGE

We could make a *DC* glow discharge by applying a potential difference between two electrodes in a gas; Figure 2.1 shows the resulting current density j flowing due to the application of a *DC* voltage V between a chromium cathode and a stainless steel anode, in argon gas at two different pressures. Each electrode was 12.5 *cm* diameter and the electrodes were 6.4 *cm* apart. Most of the space between the two electrodes is filled by a bright glow known as the negative glow, the result of the excitation and subsequent

recombination processes. Adjacent to the cathode is a comparatively dark region known as the dark space. This corresponds to the sheath formed in front of the cathode; there is a similar sheath at the anode, but it is too thin to clearly see.

DC discharges are somewhat easier to begin to analyze than *DC* discharges, although they are still extremely complex and we certainly do not understand all the details. Fortunately, much of what we learn can also be applied to *RF* systems.

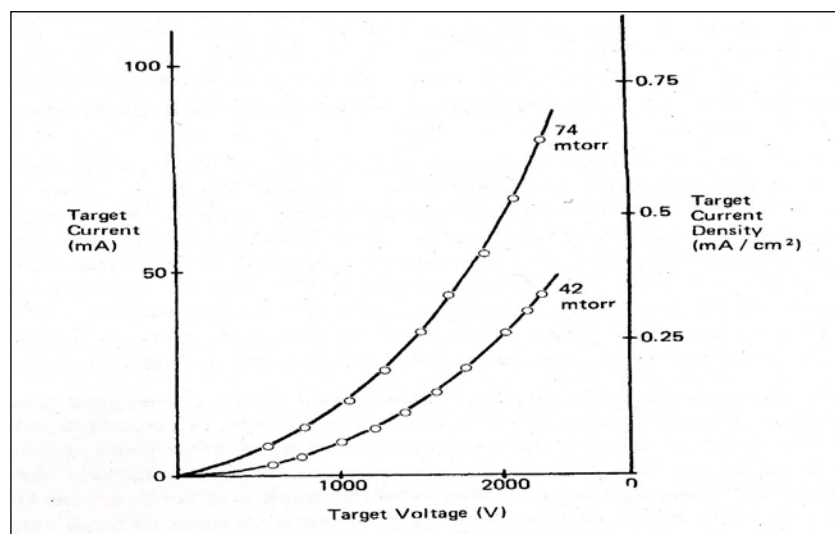


Figure 2.1. $I-V$ characteristic for Cr sputtering in argon. The figure is taken from Chapman, B.N., *Glow Discharge Processes*. The figure is taken from Chapman, B.N., *Glow Discharge Processes* [2]

Many textbooks show a whole series of glowing and dark spaces in *DC* discharges. Figure 2.2 is from Nasser [6]; virtually the same figure appears in Cobine [7], von Engel [8] and doubtlessly in many other texts. The positive column is the region of the discharge which most nearly resembles plasma and most of the classic probe studies have been made on positive columns. It is found that, when the two electrodes are brought together, the cathode dark space and the negative glow are unaffected whilst the positive column shrinks. This process continues so that eventually the positive column, and then the Faraday dark space, is 'consumed', leaving only the negative glow and dark spaces adjacent to each electrode. This last situation is the usual case in glow discharge processes as shown Figure 2.3, where the inter-electrode separation is just a few times the cathode dark space

thickness. The minimum separation is about twice the dark space thickness; at less than this, the dark space is distorted and then the discharge is extinguished.

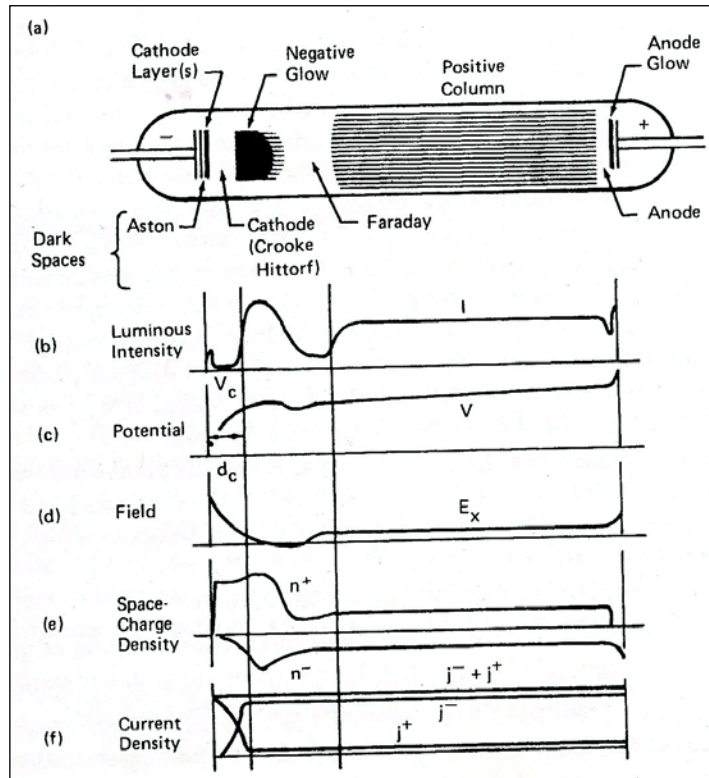


Figure 2.2. The normal glow discharge in neon in a 50 cm tube at $p = 1$ Torr. The figure is taken from Chapman, B.N., Glow Discharge Processes [2]

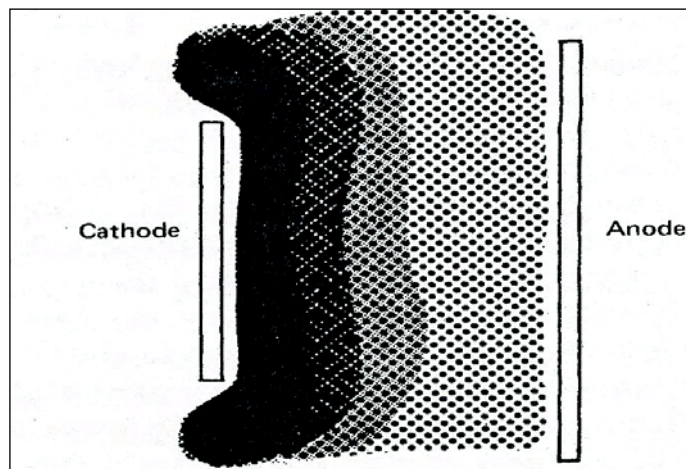


Figure 2.3. DC glow discharge process. The figure is taken from Chapman, B.N., Glow Discharge Processes [2]

Since current must be continuous in a system, it is clear that the currents at the two electrodes must be equal. In this particular system, the only other grounded electrode was remote from the discharge and had a small surface area; thus, the current densities at the chromium cathode and stainless steel anode were approximately equal. Take a typical datum point, which might be 2000 V and 0.3 mA/cm^2 at 50 mTorr . This represents an electron current density to the anode that is much smaller than the random current density $1/4 en_e \bar{c}_e$ and so there must be a net decelerating field for electrons approaching the anode, i.e. the plasma is more positive than the anode. But there is still some electron current flowing, so apparently the anode is more positive than floating potential. We earlier calculated a 'reasonable' floating potential 15 V less than the plasma potential and this is consistent with commonly found values of $V_p : 10\text{ V}$ (with respect to a grounded anode) in *DC* sputtering systems.

The plasma is virtually field-free, as we saw earlier, so the plasma has the same potential V_p adjacent to the sheath at the cathode. But the cathode has a potential of -2000 V , so the sheath voltage is $(2000 + V_p)$, i.e. -2010 V in our example Figure 2.4. Notice some peculiarities about this voltage distribution:

1. The plasma does not take a potential intermediate between those of the electrodes, as might first be expected. This is consistent with our earlier contention that the plasma is the most positive body in the discharge.
2. The electric fields in the system are restricted to the sheath at each of the electrodes.
3. The sheath fields are such as to repel electrons trying to reach either electrode.

All of these peculiarities follow from the mass of the electron being so much less than that of an ion. The third, in particular, is illustrative of the role played by electrons in a discharge.

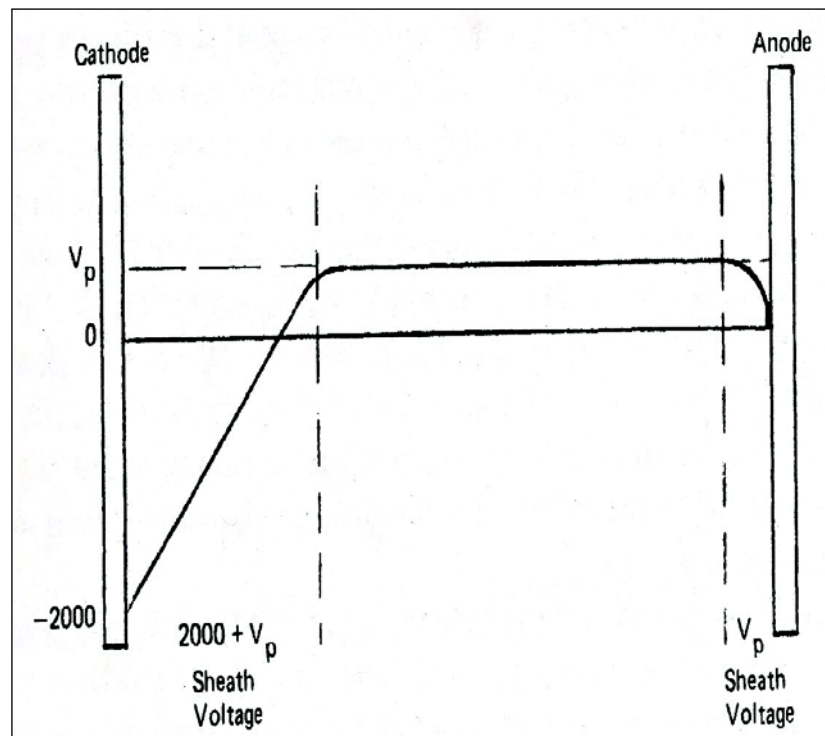


Figure 2.4. Voltage distribution in a *DC* glow discharge process. The figure is taken from Chapman, B.N., *Glow Discharge Processes* [2]

2.2. MAINTENANCE OF THE DISCHARGE

Electrons and ions are lost to each of the electrodes and to all other surface within the chamber. The loss process include electron-ion recombination (which takes place primarily on the walls and anode due to energy and momentum conservation requirements), ion neutralization by Auger emission at the target and an equivalent electron loss into the external circuit at the anode. To maintain a steady state discharge, there must be a good deal of ionization going on in the discharge.

There is also a considerable energy loss from the discharge. Energetic particles impinge on the electrodes and walls of the system, resulting in heating there; this energy loss is then conducted away to the environment. So another requirement for maintaining the discharge is that there is a balancing energy input to the discharge.

How are these ionization and energy requirements satisfied? The simplest answer is that

the applied electric field accelerates electrons, so that the electrons absorb energy from the field, and that the accelerated electrons acquire sufficient energy to ionize gas atoms. So the process becomes continuous. But that is a very simple answer and raises various other questions. Where does most ionization take place and what are the major processes involved? Can the model of the discharge that we have been developing account for the amount of ionization required? To what extent is the *DC* discharge like the plasma.

In trying to decide where most ionization occurs, the glow region must be an obvious candidate. Ionization and excitation are rather similar processes. Their thresholds and cross-section energy dependences are not so different, so that for electrons with energies well above threshold, ionization and excitation will be achieved in a rather constant ratio; as the electron energy decreases towards threshold, then excitation will occur in an increasing proportion since it has a lower threshold. So we would expect that excitation, and subsequent emission from de-excitation, will always accompany ionization—at least for the glow discharges we are considering. Hence the choice of the glow region as the prime candidate for the main ionization region. But if we look in the literature, then we often find descriptions of glow maintenance that rely entirely on ionization in the cathode sheath region. So apparently there is some disagreement over this matter.

We examine a practical *DC* discharge by dividing the discharge into three regions: the cathode region, the glow itself, and the anode region. We shall be looking not only at the ionization, but also at practical matters such as charge exchange collisions in the sheath which have the important effect of controlling the energy of bombarding ions at the cathode—important in practical applications. But before looking at these three regions, let us focus on the secondary electron emission.

2.3. SECONDARY ELECTRON EMISSION

When a particle strikes a surface, one of the possible results is that an electron is ejected. The number of electrons ejected per incident particle is called the “secondary electron coefficient” or “yield”. Secondary electron emission is observed for bombardment by ions, electrons, photons and neutrals (both ground state and metastable); each will have a different coefficient and a different energy dependence.

2.3.1. Electron Bombardment

The emission of electrons due to electron impact has been closely studied because of its importance in valves, cathode ray tubes and electron multipliers. By looking at the energy dependence of the emitted electrons in Figure 2.5, it appears that some of the bombarding electrons are elastically scattered and that some 'true' secondaries are also emitted. The 'true' secondaries are frequently, but not always, more numerous than the scattered primaries. Electron bombardment process will be significant at the anode and at walls; there is no electron bombardment at the cathode. The yield due to electron impact is usually given the symbol δ , which depends on the energy of the bombarding electron, and is typically unity for clean metals as shown Figure 2.6. However, δ is also strongly dependent on the presence of contamination or surface adsorbed layers and is higher for insulating materials. In glow discharge process, we have to deal with electron bombardment at low energies of a few V (and also some by high energy electrons) so we would really like some δ data at correspondingly low energies, but it does not seem to be too readily available.

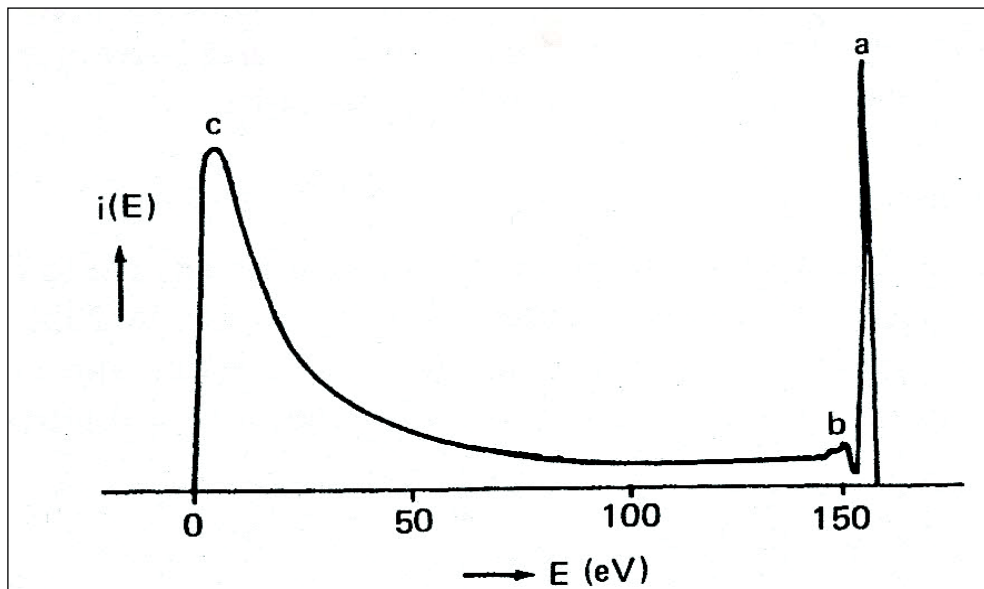


Figure 2.5. The energy distribution of secondary electrons emitted by *Ag* [9, 10], a. elastically reflected primaries, b. inelastically reflected primaries, c. 'true' secondaries.

The figure is taken from Chapman, B.N., *Glow Discharge Processes* [2]

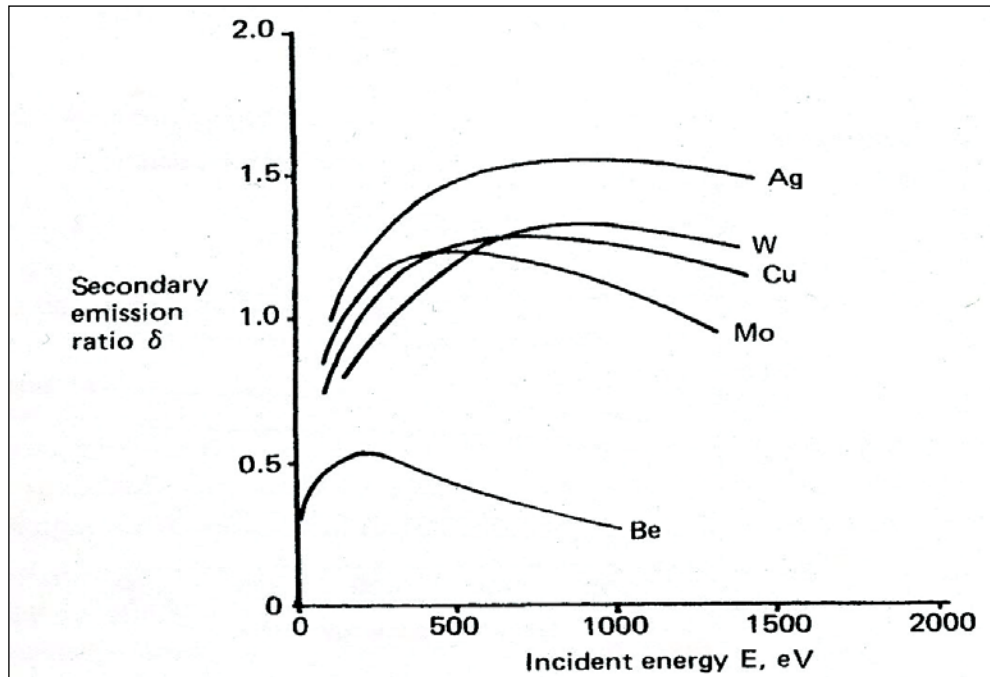


Figure 2.6. Secondary electron coefficient γ_i of different metals as a function of the energy of incident electrons [11]. The figure is taken from Chapman, B.N., Glow Discharge Processes [2]

2.3.2. Ion Bombardment

The corresponding secondary electron emission coefficient for ion bombardment is given the symbol γ_i . The energy dependence of γ_i for noble gas ions on tungsten and molybdenum is shown in Figure 2.7 and for various other ion-metal combinations in Figure 2.8. The yield is again very dependent on the condition of the surface: Figure 2.9 shows how γ_i depends on the crystal face exposed and Figure 2.10 [12] shows how the yield of polycrystalline tungsten decreases from the clean metal value on exposure to nitrogen, reaching a new quasi-steady state after about 10 minutes, coinciding with the completion of the first monolayer coverage of the nitrogen. (Note also in Figure 2.10 that the ion bombardment energy is only 10 eV, so that γ_i is still quite high in this case, even at such low ion energies). The effect of surface contamination is again shown in Figure 2.11, this time for argon ion bombardment of tungsten.

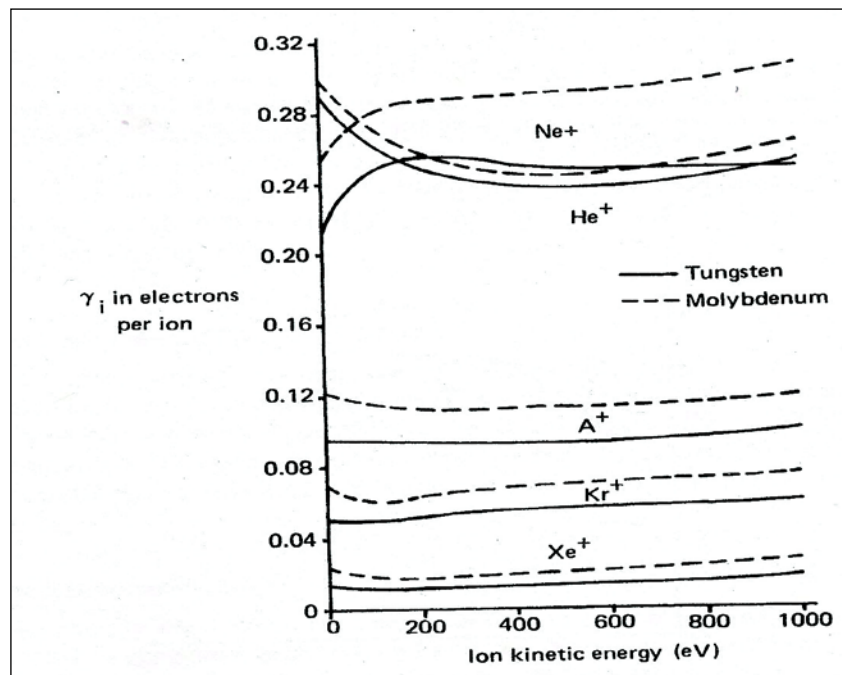


Figure 2.7. Secondary electron yields γ_i for noble gas ions on atomically clean W and Mo.

The figure is taken from Chapman, B.N., Glow Discharge Processes [2]

These variations of yield γ_i with surface condition are quite important in dc sputtering where the magnitude of the yield plays a role in determining the $V - I$ characteristics of the discharge. A sputtering target is immediately contaminated on exposure to the atmosphere, commonly with the formation of an oxide surface layer on metal targets. When the target is subsequently sputtered, there is a period when $V - I$ characteristic is continuously changing as the surface layer is removed.

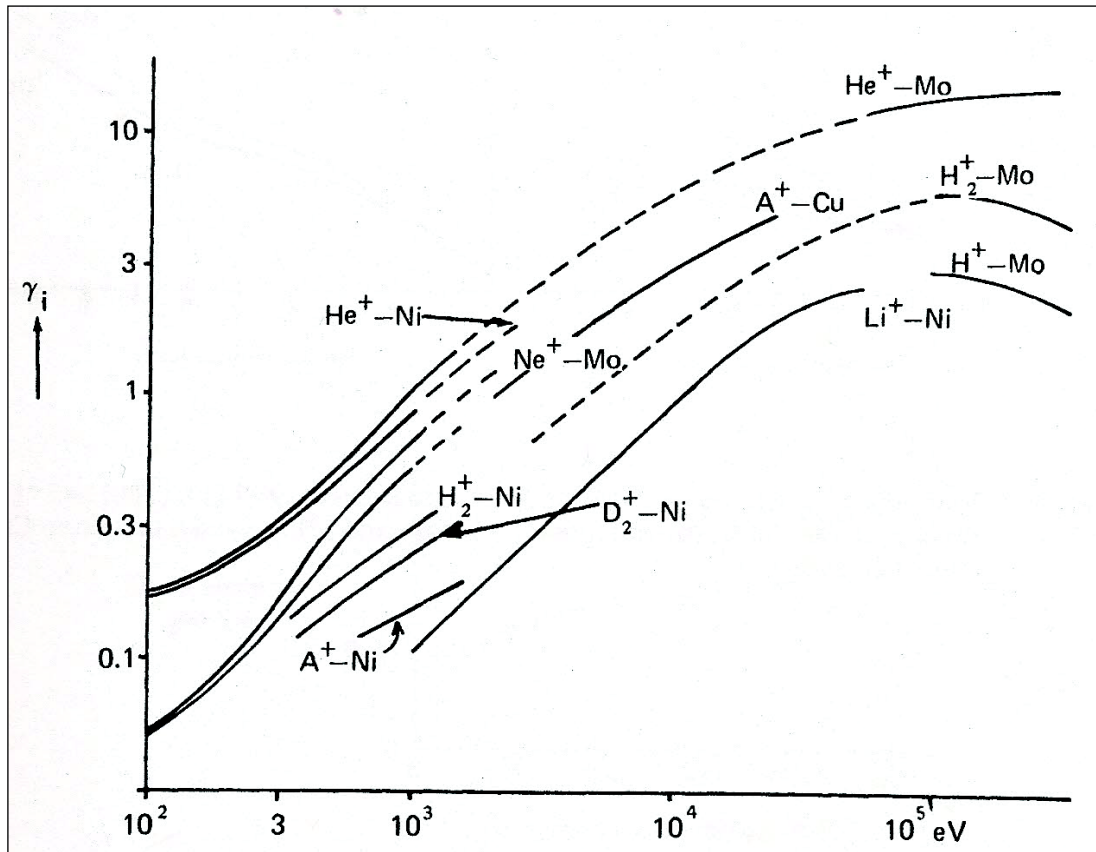


Figure 2.8. Secondary electron coefficient γ_i for ions of energy K falling on the surface of various substances [8]. The figure is taken from Chapman, B.N., Glow Discharge Processes [2]

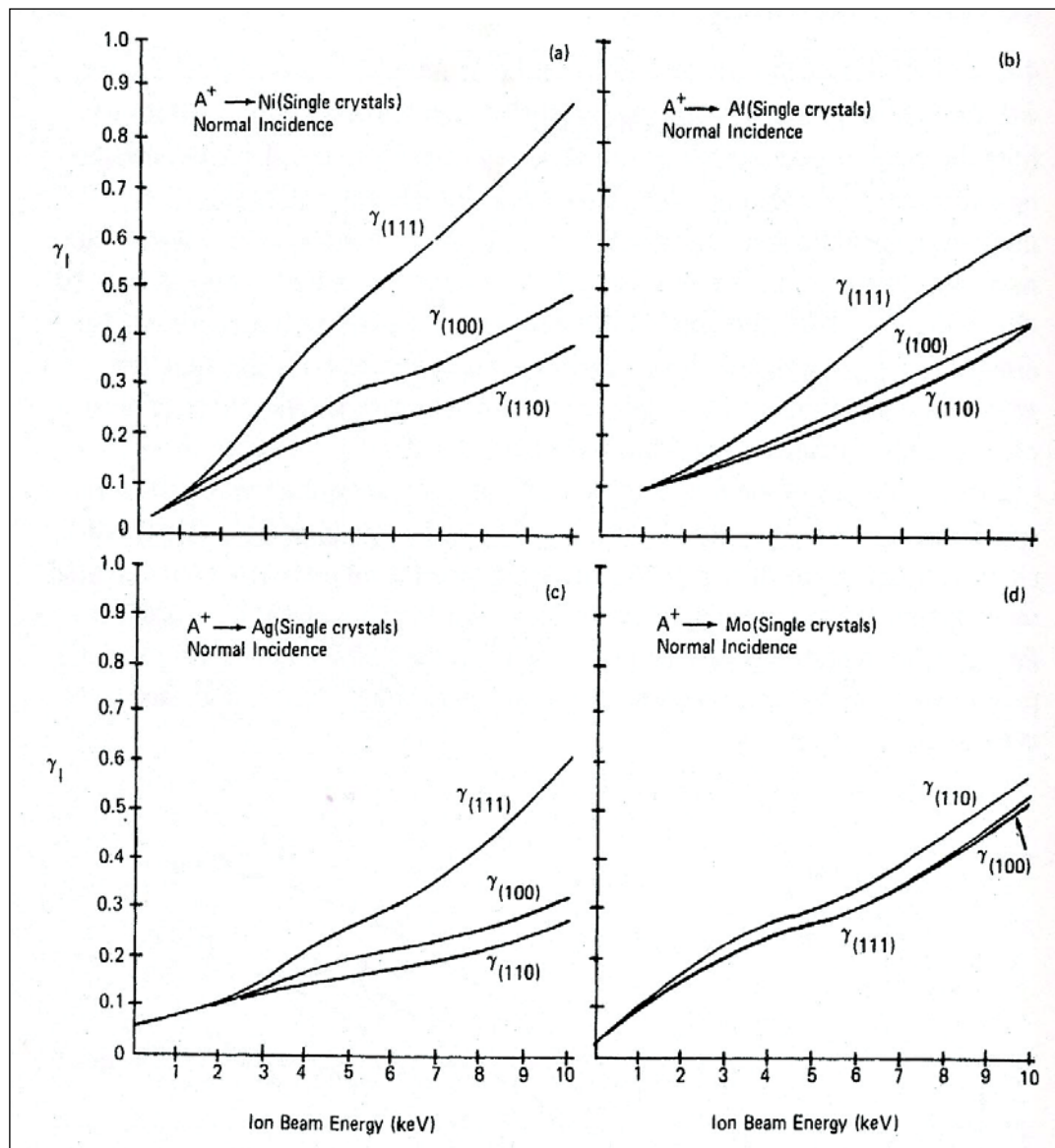


Figure 2.9. Variation of γ_i with ion energy for Ar^+ bombardment of (1 1 1), (1 0 0) and (1 1 0) surfaces of a. *Ni*, b. *Al*, c. *Ag* and d. *Mo* [8]. The figure is taken from Chapman, B.N., Glow Discharge Processes [2]

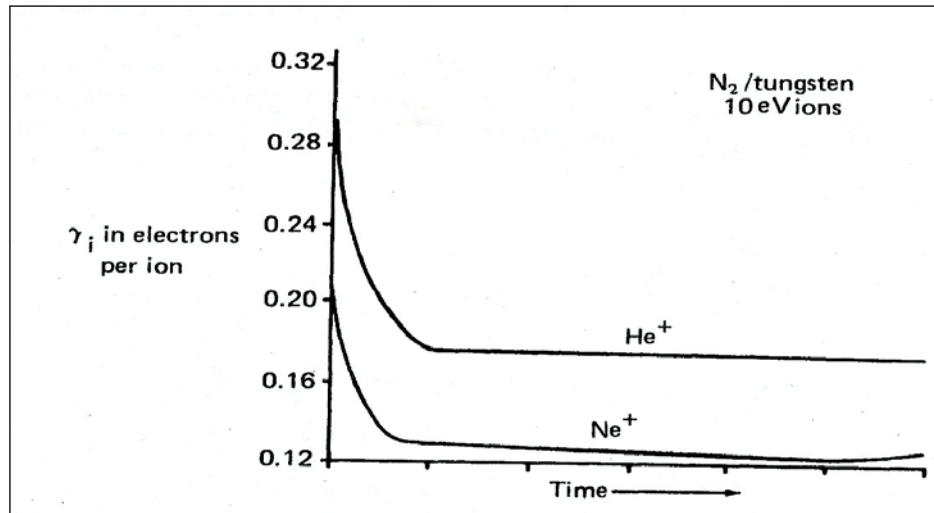


Figure 2.10. Secondary electron yields γ_i for He^+ and Ne^+ ions, as a monolayer of N forms on W . The break in the plot represents the completion of the first monolayer [13].

The figure is taken from Chapman, B.N., Glow Discharge Processes [2]

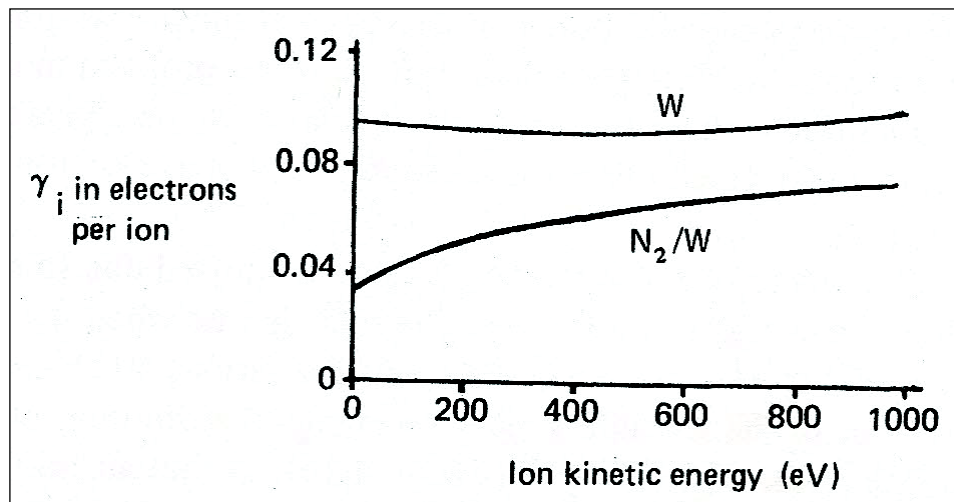


Figure 2.11. Secondary coefficient γ_i for argon ions on clean tungsten W and W covered with a monolayer of N [13]. The figure is taken from Chapman, B.N., Glow Discharge

Processes [2]

In glow discharges, ion energies on targets and substrates range from a few eV up to a few hundred eV , and so the secondary electron yield data over the corresponding range are the most useful for our investigation.

2.3.3. Neutral Bombardment

In the sheath at an electrode, energetic ions frequently collide with neutrals either elastically or with charge exchange in either case giving rise to energetic neutrals. If sufficiently energetic, these neutrals can cause secondary electron emission. Figure 2.12 shows the yields for argon ions and argon neutrals on molybdenum. It appears that there is a potential energy component for the ions only. Unfortunately, there is rather little of these data available; Figure 2.12, if typical, suggests that electron emission due to neutrals is rather unimportant in glow discharge processes where neutral energies are a few hundred eV at most.

There are likely to be long-lived metastable neutrals, particularly in noble gas discharges. Although these metastables cannot be accelerated by electric fields, being neutral, they will receive energy by collision with energetic ions, the energy transfer function making this an efficient process. Since the metastables have some potential energy, they will presumably be somewhat more effective in producing secondary electrons than their corresponding ground state parents. There seems, however, to be rather little quantitative information available.

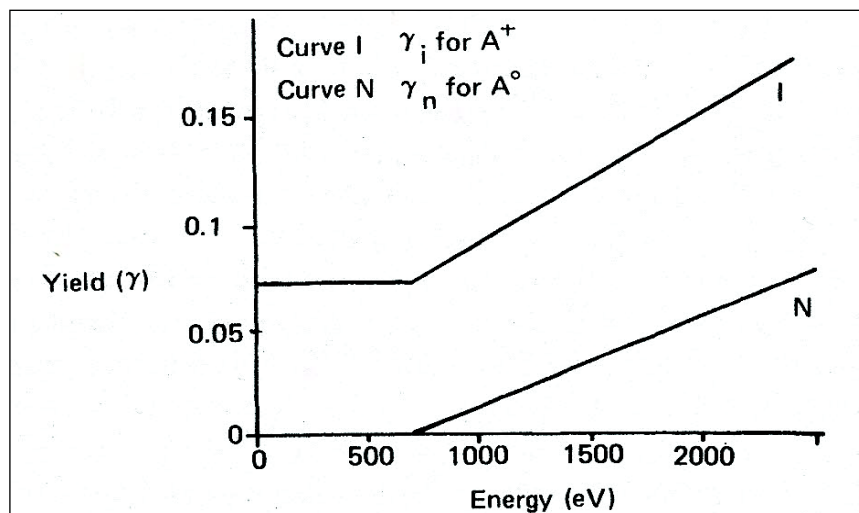


Figure 2.12. Secondary electron emission as a function of energy for Ar ion and neutral atom bombardment of Mo [14]. The figure is taken from Chapman, B.N., *Glow Discharge Processes* [2]

2.3.4. Photon Bombardment

The ejection of electrons due to photon bombardment is well-known, and is usually referred to as photoemission. For pure metals, the photoelectric yield γ_p depends on the work function ϕ of the metal, with a threshold for emission of $hc/\lambda = E$. The photoelectric yields for most pure metals are only 10^{-4} to 10^{-3} electrons per photon in the visible to near ultraviolet frequencies, largely because the photon is usually efficiently reflected, except at very short wavelengths where a corresponding increase in photoelectric yield is seen, as in Figure 2.13. There does not seem to have been much consideration of the effect of photons in sputtering and plasma etching glow discharges. It does not seem that, under the right circumstances, photoelectric yields can be as large as ion yields and certainly there are believed to be strong photon effects in rather specific cases such as hollow cathode sources. Holmes and Cozens [15] proposed a contribution from photoelectric emission in their rather high current density mercury discharge (in which they also make the rather interesting observation of a pressure gradient near the target, believed to be due to the strong ion flux there). But on the whole, the effects of photoelectric emission and photoionization in glow discharges are not well understood.

These processes are important in glow discharge processes because each of them can contribute electrons to the discharge and help to counter electron loss processes. Since the plasma is more positive than the potential of any surface in the discharge, the action of the sheath is to accelerate electrons from the surface into the glow, giving both electrons and energy to the discharge.

Our practical processes result in surface bombardment energies from a few eV up to several hundred eV or even a few thousand eV and we need, therefore, to consider secondary electron data over this range. Ion bombardment will clearly be of importance at the cathode of a DC discharge and both electron and ion bombardment at the anode. The importance of metastable and ground state neutrals and of photons, has to be further assessed.

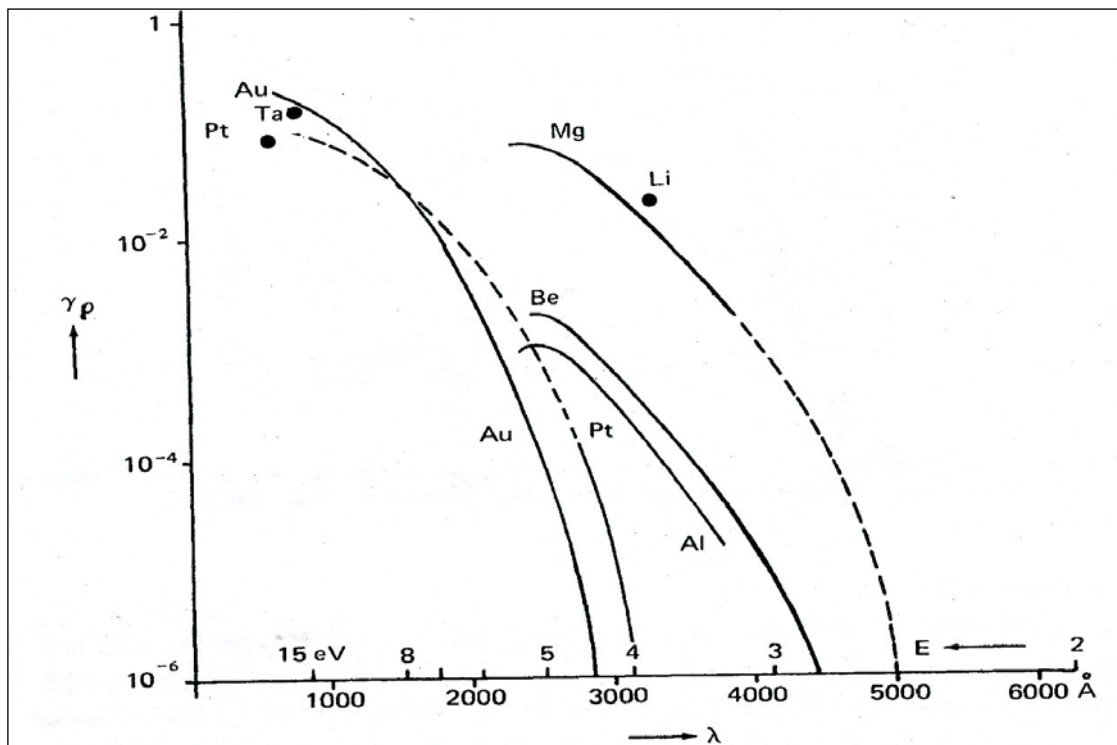


Figure 2.13. Photoelectric yield γ_p as a function of the wavelength λ of the incident light (energy E of quantum) for various substances [8]. The figure is taken from Chapman, B.N., Glow Discharge Processes [2]

The detail of the loss process for electrons and ions at electrodes and walls is complicated by secondary electron emission from those surfaces. When we have previously looked at currents to surfaces, e.g. in "Sheath Formation at a Floating Substrate", we have tacitly ignored the effects of secondary emission, which would change the net current to a surface or modify its floating potential, for example.

2.4. THE CATHODE REGION

The type of *DC* discharge used in glow discharge processes is known as an abnormal glow discharge. At lower applied voltages and consequent lower currents, a discharge can result which is characterized by constant voltage and constant current density. This is a normal glow discharge. More power applied to the system is manifested by an increase in the size of the region of the cathode carrying current (j and V remaining constant) until the whole cathode is utilized, at which stage the discharge becomes abnormal.

The cathode plays an important part in *DC* sputtering systems because the sputtering target actually becomes the cathode of the sputtering discharge. The cathode is also the source of secondary electrons and these secondary electrons have a significant role both in maintaining the discharge and in influencing the growth of sputtered films.

When the formation of sheaths was being considered, we made the assumption that there were no collisions in the sheath. Many books and papers on plasma physics are concerned specifically with collisionless plasmas, but this is because most current interest is in plasmas which have very high temperatures of many *keV* and these are essentially collisionless; such plasmas are of interest in fusion. 'Our' plasmas are very different and do have lots of collisions, both in the sheaths and in the glow.

In trying to understand the mechanism by which a discharge is sustained, it is clearly necessary to account for all the recombination and energy loss processes which occur in Figure 2.14. We could simplify the situation for purposes of analysis by considering a discharge between very large electrodes close together, which is usually the case in high pressure planar diode plasma etchers and some sputter deposition systems.

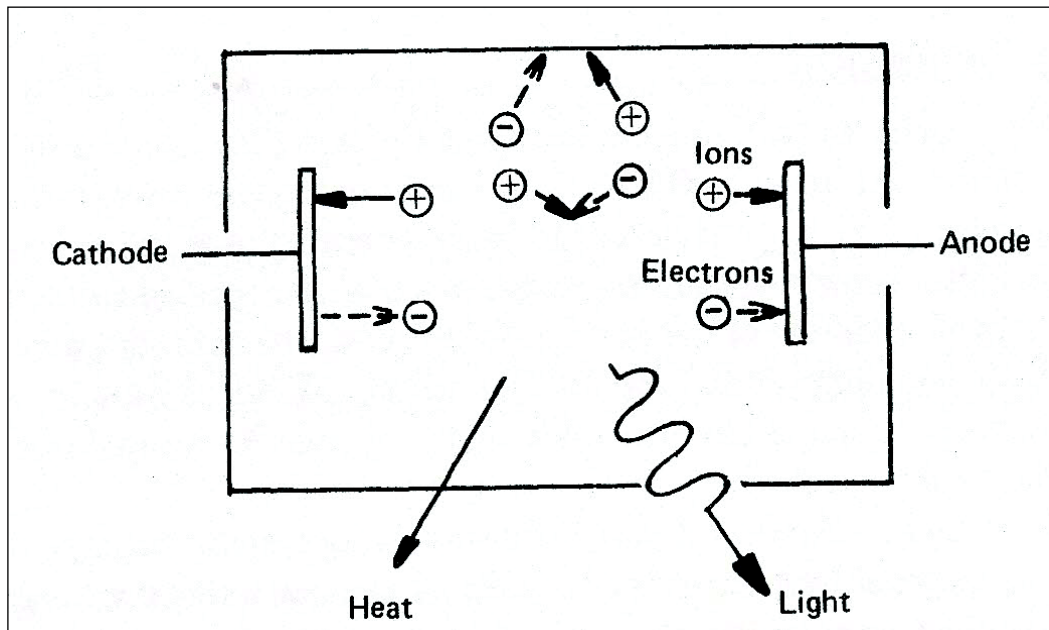


Figure 2.14. Discharge loss processes. The figure is taken from Chapman, B.N., *Glow Discharge Processes* [2]

2.4.1. Ionization in the Sheath

Some descriptions of the glow discharge rely on ionization caused by secondary electrons from the target as they are accelerated across the dark space in Figure 2.15. This can be modelled by considering the amount of ionization caused by a flux $N_e(x)$, electrons passing through a thin slab of thickness Δx located at x from the cathode as shown Figure 2.16. The density of neutrals is n and the ionization cross-section (assumed energy-independent for simplicity) is q .

Number of ionizing collisions is equal to $N_e(x)nq\Delta x$, thus

$$\frac{dN_e(x)}{N_e} \Delta x = N_e(x)nq\Delta x \quad (2.1)$$

$$\int \frac{dN_e}{N_e} = \int nq dx \quad (2.2)$$

$$N_e(x) = N_e(0)\exp(nqx) \quad (2.3)$$

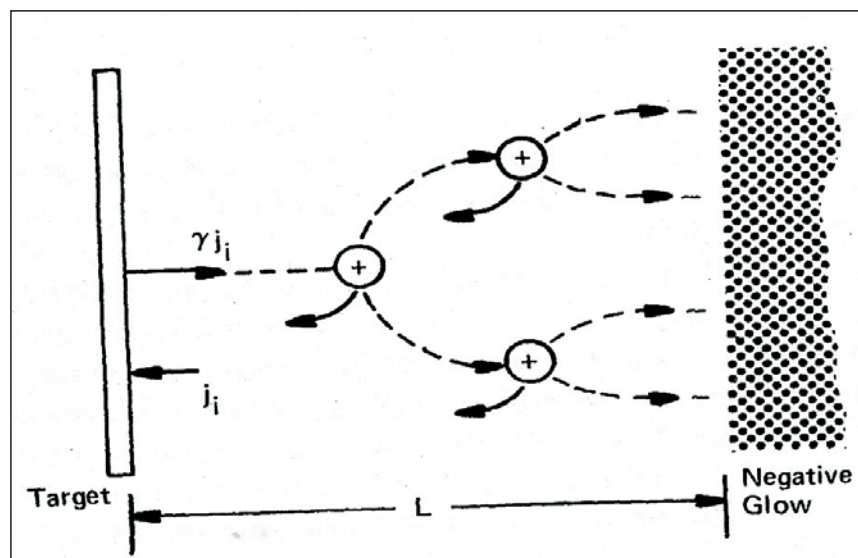


Figure 2.15. Ion pair production in the dark space. The figure is taken from Chapman, B.N., Glow Discharge Processes [2]

Therefore each electron that leaves the target is multiplied by $\exp(nqL)$ by the time it reaches the edge of the dark space. The electric field in this region is strong enough that the major part of the electron travel will be straight across the dark space along the field lines.

Let us obtain an idea of the magnitude of this electron multiplication for the practical conditions under consideration. We found before that the maximum ionization cross-section for electrons in argon is $2.9 \times 10^{-16} \text{cm}^2$ for 100 eV. Davis and Vanderslice [16], whose work on collisions in the sheath we shall be considering shortly, found a sheath thickness of 1.3 cm for a discharge voltage of 600 V in argon at 60 m Torr, for which $n = 2.1 \times 10^{15}$, using a Kovacs alloy cathode. These figures put an upper limit on electron multiplication of $\exp(2.1 \times 10^{15} \times (2.9 \times 10^{-16} \times 1.3)) = 2.2$.

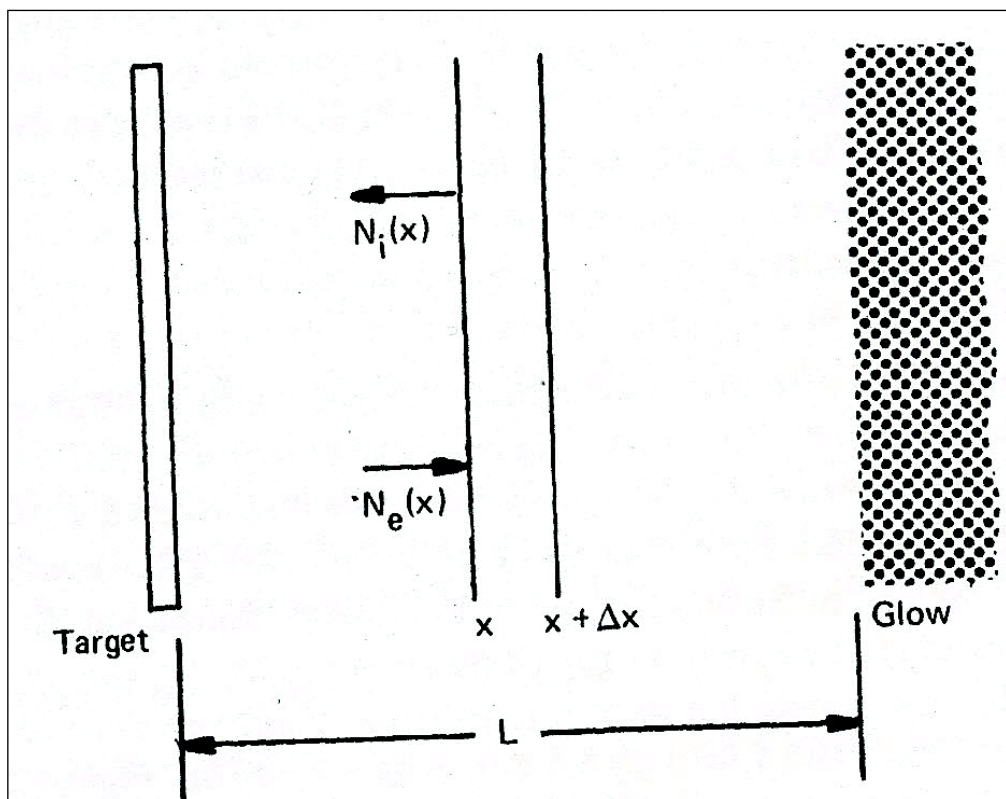


Figure 2.16. Analysis of ion pair production in the dark space. The figure is taken from Chapman, B.N., Glow Discharge Processes [2]

For each ionization, a new ion is formed as well as a new electron. For each electron that

leaves the target, $\exp(nqL - 1)$ ions will be formed. For each ion that strikes the target, γ secondary electrons will be emitted, where γ is the sum yield for all of the various processes. Hence, each ion that strikes the target will lead to the generation of $\gamma(\exp(nqL - 1))$ ions within the dark space. The yield γ is unlikely to exceed 0.2 for most metals, and this suggests an ion production rate of 0.244 ions per ion; remember that this is an upper limit based on the use of the maximum cross-section for ionization in argon.

2.4.2. Structure of the Cathode Sheath

Let us account for the large difference between the Debye length and typical cathode sheath dimensions. In the subsequent derivation of the potential distribution around the perturbation, we assume that the ion density remained constant at its unperturbed value. But as we have just seen, a large semi-permanent negative potential causes the formation of a positive space charge sheath of varying density. This sheath may be as much as a few cm thick. Our final sheath model Figure 2.17 therefore has 3 regions:

1. A quasi-neutral *pre-sheath* in which ions are accelerated to satisfy the Bohm criterion.
2. A region of the extent of a few Debye lengths in which the electron density rapidly becomes negligible.
3. A region of space charge limited current flow, which would be of zero electron density in the absence of secondary electron emission from the target, and in practice is not so different because of the rapid acceleration of the electrons.

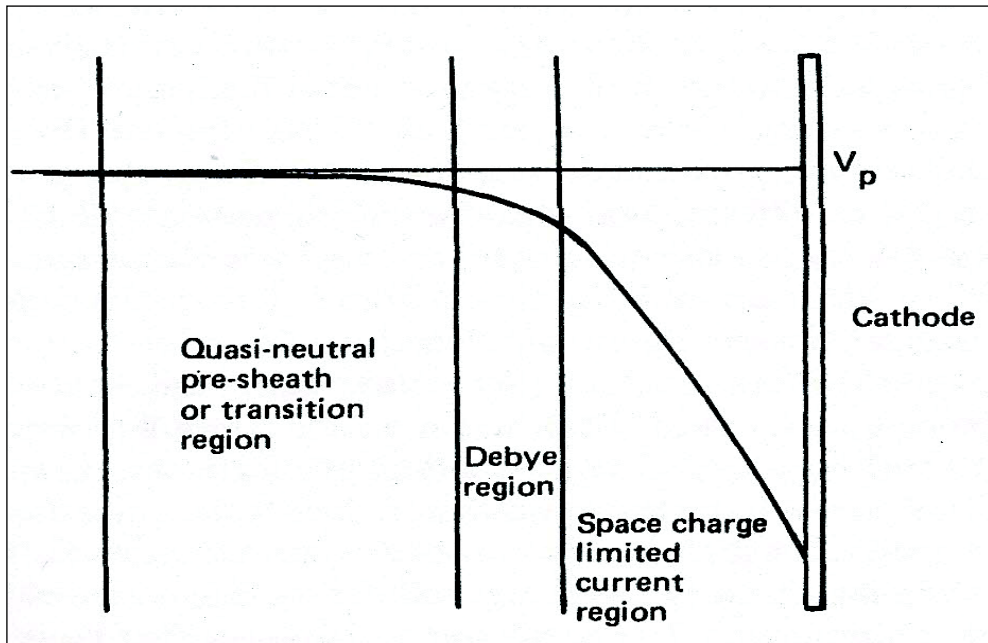


Figure 2.17. Regions of a cathode sheath. The figure is taken from Chapman, B.N., Glow Discharge Processes [2]

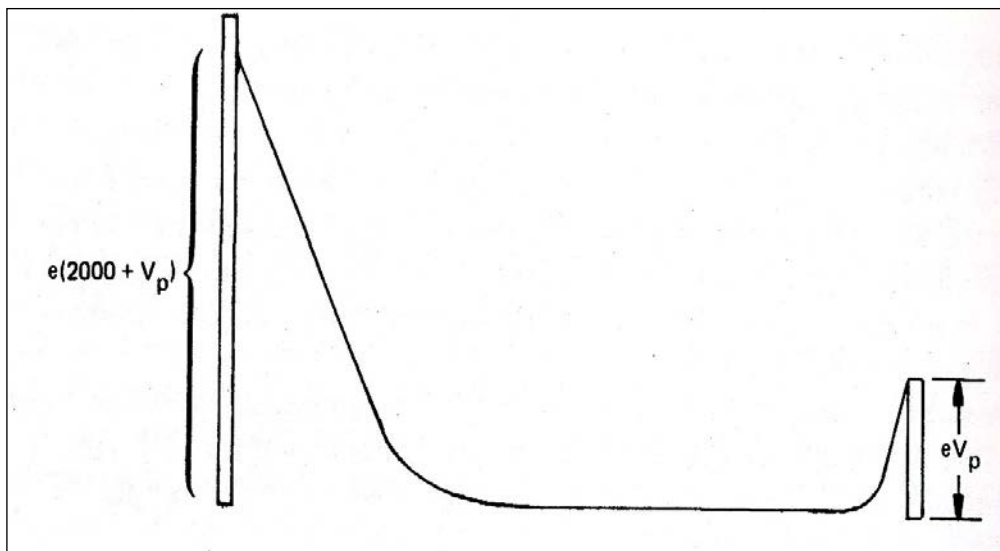


Figure 2.18. Electron energy diagram for the *DC* glow discharge. The figure is taken from Chapman, B.N., Glow Discharge Processes [2]

Note that these divisions are in our minds only. A difficulty in experiments on sheath thicknesses is of trying to decide where the edge of the sheath is. Practically, people generally look for the change of luminous intensity due to de-excitation, either with a

travelling microscope or an emission spectrometer with spatial resolution. But a change in intensity need not necessarily coincide with the boundary of the sheath as we have defined it. Fortunately, since the average thermal velocity of excited atoms will be about $5 \times 10^4 \text{ cm/sec}$, at least we do not generally have to worry about atoms moving appreciably between excitation and relaxation, which might not be the case for excited ions in the sheath or excited sputtered atoms, which have greater than thermal energies.

2.4.3. Application to Glow Discharge Sheaths

Which one of these space charge limited current equations applies to the sheaths in our discharges? The first problem is that the equations were derived for single charge carriers and we have two-electrons and ions (and even more if multiple ions are included). Actually this is not much of a problem because the electrons accelerate away from the sheath so rapidly that they produce a very small space charge density. However, the assumption that negligible electron density would not be true if there were copious ionization in the sheath.

Let us see what order of current densities are predicted by the two space charge equations. We will use again the example from the data of Davis and Vanderslice a 600 V sheath of thickness 1.3 cm , in argon so that m is $6.6 \times 10^{-26} \text{ kg}$. Substituting these values into the collisionless Child-Langmuir equation, we obtain a value of $75 \mu\text{A/cm}^2$. This seems quite low, at the bottom end of the values obtained in sputtering systems. But 600 V is quite a low cathode voltage for a *DC* sputtering system. Unfortunately Davis and Vanderslice do not report the current they obtained for this condition, but they do for another situation- 30 mA current from a 500 V sheath of thickness 0.18 cm at 500 mTorr . For these conditions the high vacuum current would be 2.9 mA/cm^2 ; since their target was 4.5 cm diameter, their actual current density was 1.9 mA/cm^2 . The difference could well have been due to the charge exchange collisions in the sheath.

To use another example, Güntherschulze (1930) report values for a helium discharge with an iron cathode, equivalent to a dark space thickness of 0.64 cm at 1 Torr for a voltage of 1000 V . The high vacuum space charge density should then be equal to 2.1 mA/cm^2 , which compares very well with the measured value of 2 mA/cm^2 . The good agreement may be fortuitous, although the charge exchange cross-section for He^+ in He is several

times lower than the equivalent figure for argon. Returning to argon, we should note that a 1000 V sheath of thickness 1 cm would give a current density of 0.27 mA/cm^2 ; all of these values are consistent with observed sputtering values. We cannot expect to achieve very precise values of the space charge limited current because of the difficulties involved in assessing L . However, it does seem that the observed cathode currents are almost as large as the values predicted by the collisionless Child-Langmuir equation. This implies either that the saturation value of ion current from the glow has not been reached, or that the sheath thickness adjusts itself to extract precisely the saturation current. It would be difficult to test this in a diode discharge because increasing the cathode voltage would increase the power input to the discharge. The high voltage probe characteristics might be more illuminating. Tisone and Cruzan (1975) have measured the target voltage and sheath thickness for a target immersed in a hot filament discharge. They obtained rather good agreement with a $V \propto x^{4/3}$ relationship. It seems as though the sheath thickness is determined by the ion production rate in the glow and by the space charge limitation, at least in this case.

A second implication of the small differences between the free fall current limit and the measured values is that there are not many collisional processes in the sheath involving ions. This is further evidence that there is not much ionization in the sheath.

By definition, any motion in the sheath that is not free-fall is mobility limited, though not generally with the simple field-independent mobility μ assumed in the derivation of the mobility limited space charge equation. This is common practice when looking at conduction in gases at lower fields and higher pressure: even then μ is very dependent on ϵ , as can be seen from the data presented. Note that ϵ/p is typically around a few *volts/cmTorr* in these example (although up to 100 and 240 *volts/cmTorr* in two untypical cases). By comparison, our earlier example of a 500 V sheath of thickness 0.18 cm at 500 *mTorr* corresponds to ϵ/p values increasing from about 0 at the sheath-glow interface up to $1.11 \times 10^4 \text{ V/cmTorr}$ at the cathode, if we follow the assumptions of Davis and Vanderslice [16]. Obviously we can predict the observed values by suitably choosing μ , which in this example would need to be $446 \text{ cm}^2/\text{voltsec}$. If we guess, at an average argon ion arrival energy at the cathode of 100 eV, then this is equivalent to a velocity of $2.1 \times 10^6 \text{ cm/sec}$. The field at the cathode in this example is

predicted to be $5.6 \times 10^3 V/cm$, so this gives a crude estimate of μ equal to $375 cm^2/voltsec$. Mobility figures obtained in these two ways are virtually forced to agree, but the consistency is encouraging. The main point, however, is that these mobility figures are more than two orders of magnitude higher than equivalent figures obtained for conventional mobility limited situations. We can therefore conclude that ion motion in the sheaths of our *DC* discharges is much closer to free fall than conventional mobility limitation.

Finally, we should note that since the product of sheath thickness and pressure in *DC* system is observed to be constant, then reducing the operating pressure will not significantly change the number of collisions in the sheath. By the same token, neither will increasing the pressure and ion motion will remain closer to free fall than mobility limited. Hence the earlier comment that the title of high pressure space charge equation for the mobility limited situation was rather misleading. We can change the situation in *RF* system which retain sheath thicknesses of about $1 cm$ even when the pressure is reduced down to $1 mTorr$. At such a low pressure, collisions in the sheath become very unlikely and motion becomes essentially free-fall, albeit modulated by the applied *RF*.

2.5. THE ANODE REGION

We saw how a small sheath must be set up in front of the anode, of sufficient magnitude to repel some of the random flux $n_e c_e$ of electrons and reduce the current density at the anode to a more practical value. Our model of the sheath was essentially the same as that in front of a floating substrate except that the sheath voltage is not as large as at the anode. We need to involve a presheath or transition region to satisfy the Bohm criterion and we expect this to apply to the anode too. The anode sheath is found to be so thin, usually about an order of magnitude less than the cathode sheath, that it should be essentially collisionless- and in particular not a source of ionization, which was tenuous even in much thicker cathode sheath.

The anode sheath will not be very different from that in our derivation of Debye shielding. The Bohm criterion requires the ions to enter the sheath with an energy of about kT_e/e and they then accelerate through the anode sheath to reach energies of $10 - 15 eV$. The

energy increase of a factor of $3 - 10$ is equivalent to a velocity increase of $\sqrt{3} - \sqrt{10}$, and an inverse change in ion density. The main point is that the ion density is not far from the uniform density assumed in the Debye sheath derivation and does not vary anywhere near as much as in the cathode sheath. At the same time, the sheath voltage is small enough that the electron density does not go to zero as in the cathode sheath. The net result is that the anode sheath consists primarily of a pre-sheath and a Debye-like region.

3. PLASMA POTENTIAL

Three sets of particles exist in the plasma (ions, electrons and neutrals) varying by mass and temperature. In addition,

$$\bar{c} = \sqrt{\frac{8kT}{\pi m}} \quad (3.1)$$

The *electron density* and *ion density* are equal (on average); this number, which is much less than the density of neutrals, is often known as the *plasma density*. The average speed of the electrons is enormous compared with those of the ions and neutrals, due to both the high temperature and low mass of the electrons.

Suppose we suspend a small electrically isolated substrate into the plasma. Initially it will be struck by electrons and ions with charge fluxes, i.e. current densities

$$j_e = \frac{en_e\bar{c}_e}{4} \quad (3.2)$$

$$j_i = \frac{en_i\bar{c}_i}{4} \quad (3.3)$$

But \bar{v}_e is much larger than \bar{v}_i . For the values given in Table 3.1.

$$j_e \approx 38\text{mA/cm}^2 \quad (3.4)$$

$$j_i \approx 21\mu\text{A/cm}^2 \quad (3.5)$$

are found.

Table 3.1. Typical parameter values for a glow discharge plasma

Species	Mass (g)	Temperature (K and eV)	Velocity (cm/s)
Neutrals	6.6×10^{-23}	293 K = 0.025 eV	4.0×10^4
Ions	6.6×10^{-23}	500 K = 0.04 eV	5.2×10^4
Electrons	9.1×10^{-28}	23200 K = 2 eV	9.5×10^7

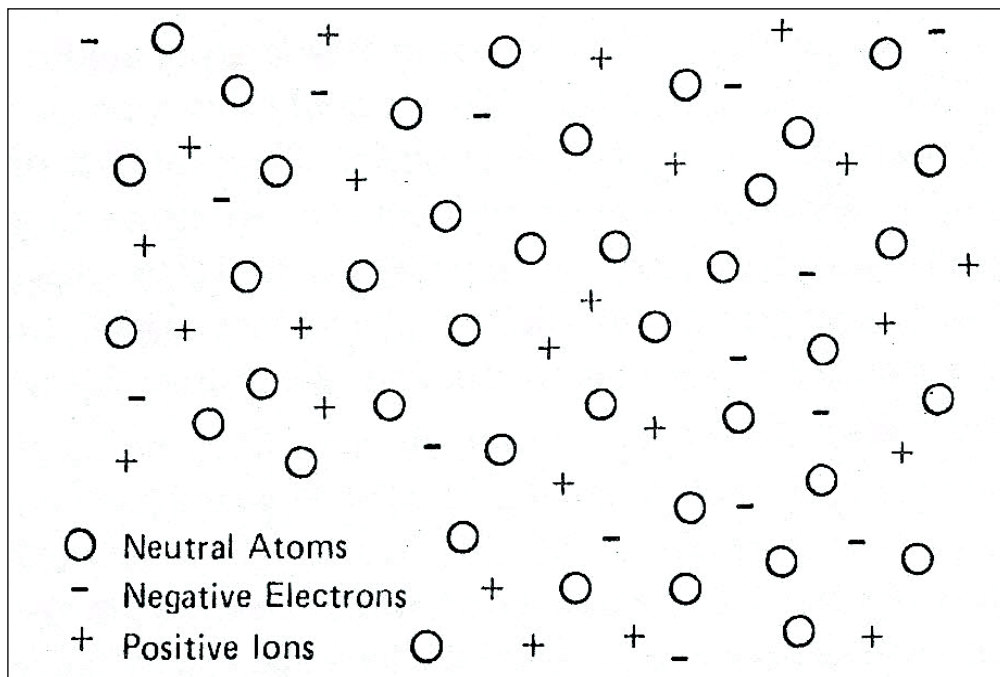


Figure 3.1. Negative, positive and neutral atoms. The figure is taken from Chapman, B.N.,
Glow Discharge Processes [2]

Since $j_e \gg j_i$, then the substrate immediately starts to build a negative charge and hence negative potential with respect to the plasma. Immediately the quasi-random motions of the ions and electrons in the region of our subject are disturbed. Since the substrate charges negatively, electrons are repelled and ions are attracted. Thus the electron flux decreases, but the object continues to charge negatively until the electron flux is reduced by repulsion just enough to balance the ion flux. We shall show shortly that the plasma is virtually electric field free, except around perturbations and so is equipotential. Let us call this potential *plasma potential* V_p , also sometimes known as *space potential*. Similarly, we can associate a floating potential V_f with the isolated substrate. [In the case of a plasma

container having insulating walls, these walls also require zero steady state net flux, so that *wall potential* and floating potential are related terms]. Since V_f is such as to repel electrons, then $V_f < V_p$. In the absence of a reference, only the potential difference $V_p - V_f$ is meaningful. Because of the charging of the substrate, it is as though a potential energy *hill* develops in front of the substrate in Figure 3.3. However, it is a downhill journey for ions from the plasma to the substrate, but uphill for the electrons, so that only those electrons with enough initial kinetic energy make it to the *top*, i.e. the substrate.

3.1. SHEATH FORMATION AT A FLOATING SUBSTRATE

Since electrons are repelled by the potential difference $V_p - V_f$, it follows that the isolated substrate (assumed planar for simplicity in Figure 3.2) will acquire a net positive charge around it. This is generally known as a space charge and in the context of glow discharge plasmas, forms a sheath. The sheath has certain density of charges, known as the space density ρ . Poisson's equation relates variation of potential V with distance x across regions of net space charge

$$\frac{dV^2}{dx} = -\frac{\rho}{\epsilon_0} \quad (3.6)$$

This is the one-dimensional form for *MKS* units, where ϵ_0 is the permittivity of free space.

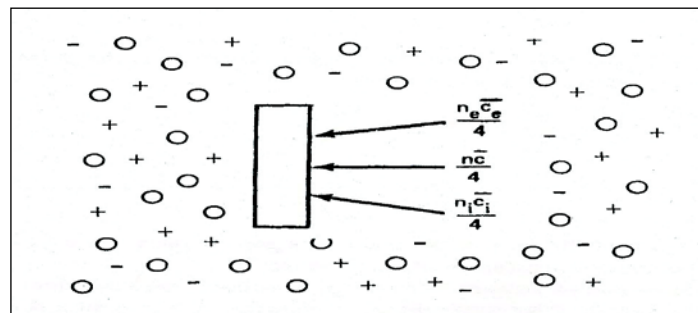


Figure 3.2. Initial particle fluxes at the substrate. The figure is taken from Chapman, B.N., *Glow Discharge Processes* [2]

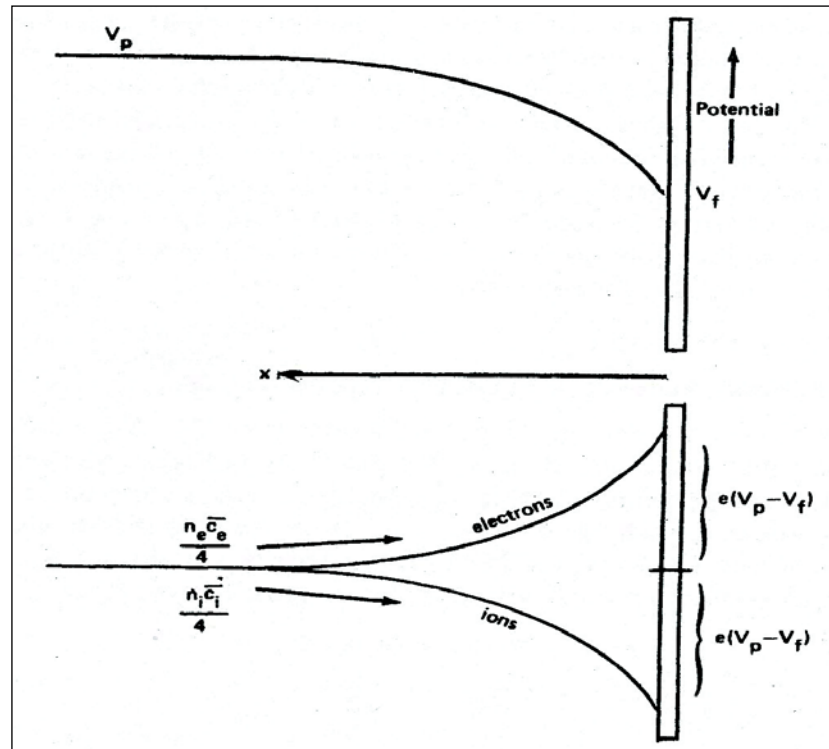


Figure 3.3. Variation of electrical potential (upper) and of the potential energies of electrons and positive ions (lower) in the vicinity of an electrically floating substrate. The figure is taken from Chapman, B.N., Glow Discharge Processes [2]

Since electric field E is given by

$$E = -\frac{dV}{dx} \quad (3.7)$$

then

$$\frac{d^2V}{dx^2} = \frac{\rho}{\epsilon_0} \quad (3.8)$$

and this just says that the electric field across a gap changes as we go through regions of net charge, consistent with experience.

If the sheath acquires a net positive charge, it follows that the electron density decreases in the sheath—we shall obtain a quantitative expression for the decrease below. But one of the

obvious features of a discharge is that it glows and as we have already seen, this is due to the relaxation of atoms excited by electron impact. So the glow intensity depends on the number density and energy of the exciting electrons. Since the electron density is lower in the sheath, it does not glow as much. So we can actually see the sheath as an area of lower luminosity than the glow itself- the substrate is surrounded by a (comparatively) dark space, a feature common to the sheath formed around all objects in contact with the plasma, even though the sheath thicknesses may vary greatly.

Let us now try to get an idea of the magnitude of $V_p - V_f$, which represents a barrier to electrons. To surmount this barrier, an electron must acquire $e(V_p - V_f)$ of potential energy as shown Figure 3.4. Hence, only electrons that enter the sheath from the plasma with kinetic energies in excess of $e(V_p - V_f)$, will reach the substrate. The Maxwell-Boltzmann distribution function tells us that the fraction n'_e/n_e that can do this is

$$\frac{n'_e}{n_e} = \exp\left(-\frac{e(V_p - V_f)}{kT_e}\right) \quad (3.9)$$

If the density n'_e just achieves charge flux balance at the object, then

$$\frac{n'_e \bar{c}'_e}{4} = \frac{n_i \bar{c}_i}{4} \quad (3.10)$$

One might at first think that the n'_e electrons close to the substrate would have a lower mean speed \bar{c}'_e than the n_e electrons in the plasma, since the n'_e electrons suffer an $e(V_p - V_f)$ loss of kinetic energy in crossing the sheath. However, one must also bear in mind that the n'_e electrons that reach the substrate were not *average* electrons, but had energies greater than the average. In fact, the average energies of the n_e and n'_e groups of electrons are the same, i.e. they are at the same temperature.

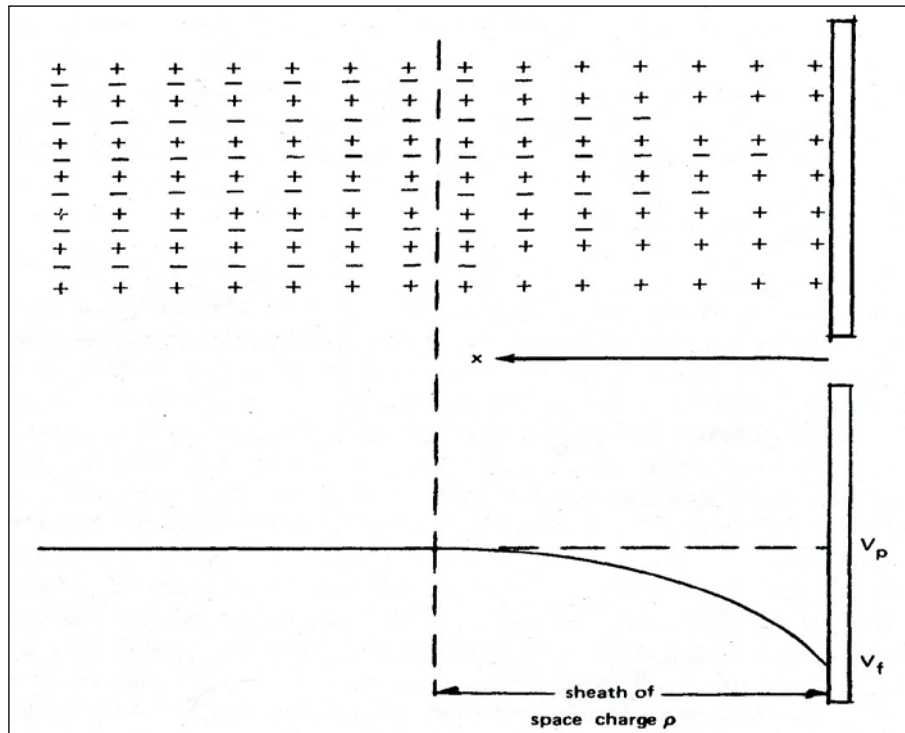


Figure 3.4. A space charge sheath develops in front of a floating substrate (upper), and establishes a sheath voltage (lower). The figure is taken from Chapman, B.N., *Glow Discharge Processes* [2]

This can be shown from the Maxwell-Boltzmann distribution which, in a region of potential energy $e\varphi$, becomes

$$dn'_e = 4\pi n_e \left(\frac{m_e}{2\pi kT_e} \right)^{3/2} c_e^2 \exp \left[-\frac{\frac{1}{2}m_e c_e^2 + e\varphi}{kT_e} \right] dc_e = \exp \left(-\frac{e\varphi}{kT_e} \right) dn_e \quad (3.11)$$

Therefore

$$\overline{c_e'^2} = \frac{\int c_e^2 \left(-\frac{e\varphi}{kT_e} \right) dn_e}{\int \exp \left(-\frac{e\varphi}{kT_e} \right) dn_e} = \overline{c_e^2} \quad (3.12)$$

Furthermore, by integration

$$n'_e = n_e \exp\left(-\frac{e\phi}{kT_e}\right) = n_e \exp\left(-\frac{e(V_p - V_f)}{kT_e}\right) \quad (3.13)$$

Returning to the charge flux balance equation, and substituting for n'_e and \bar{c}'_e then

$$n_e \exp\left(-\frac{e(V_p - V_f)}{kT_e}\right) \frac{\bar{c}_e}{4} = \frac{n_i \bar{c}_i}{4} \quad (3.14)$$

However, $n_e = n_i$ and using equation (3.2), charge balance requires

$$V_p - V_f = \frac{kT_e}{e} \ln \frac{\bar{c}_e}{\bar{c}_i} = \frac{kT_e}{2e} \ln \left(\frac{m_i T_e}{m_e T_i} \right) \quad (3.15)$$

In our example Figure 3.1, $V_p - V_f$ should have a value of +15 V volts, which is of the right order to agree with observation. Note the polarity, which is to make plasma positive with respect to the floating object, indeed, positive with respect to almost everything. The rapid motion of the electrons, relative to the ions, means they can easily move away from the plasma. But in doing so they leave the plasma more positive which hinders the escape of the negative electrons and makes the process self-limiting.

Since the charging of the floating substrate serves to repel electrons, it also attracts positive ions. This does not increase the flux of ions, which is limited by the random arrival of ions at the sheath-plasma interface-in terms of the model in Figure 3.3, it does not matter how steep or high the hill is. However, the voltage across the sheath does directly influence the energy with which the ion strikes the substrate. The ion enters the sheath with very low energy. It is then accelerated by the sheath voltage and, in the absence of collisions in the sheath, would strike the substrate with a kinetic energy equivalent to the sheath voltage.

In practice, the sheath above an electrically isolated substrate varies from 1 or 2 volts upwards. The resulting kinetic energies must be compared with inter-atomic binding energies in a thin film or substrate of typically 1 – 10 eV , so that it is easy to imagine that a growing thin film or an etching process on an electrically isolated surface in the plasma might be much affected by such impact.

3.2. PROBE CHARACTERISTICS

Consider the simple plasma of Figure 3.2. Previously we considered what would happen to an electrically isolated probe placed in the plasma. Now let us pursue further what happens when that probe is maintained at a potential V set by an external power source as shown in Figure 3.5. To make the situation more realistic, introduce a conducting wall at ground potential ($0 V$) to act as a reference voltage and as a return current path.

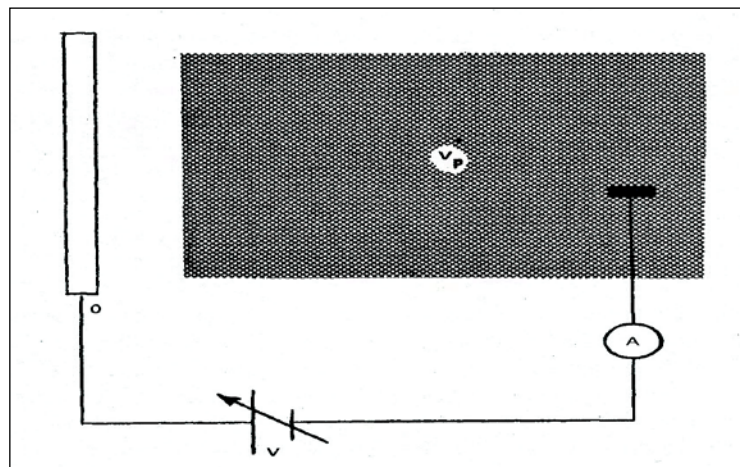


Figure 3.5. Schematic representation for measurements in a plasma. The figure is taken from Chapman, B.N., *Glow Discharge Processes* [2]

The plasma potential V_p is then defined with respect to ground. The random fluxes in the plasma are $\frac{n_e \bar{c}_e}{4}$, and $\frac{n_i \bar{c}_i}{4}$ for electrons and ions respectively. We have already seen that the net flux, and hence net current, would be zero when the probe acquires a potential V_f , the floating potential. So we can begin to plot a curve of probe current density versus probe voltage as shown in Figure 3.6. By biasing the probe negatively with respect to V_p , some electrons are prevented from reaching the probe, but the ion current density j_i remains at a value dictated by the arrival rate of ions at the edge of the sheath and this is limited to the random flux in the discharge, i.e. $n_i \bar{c}_i/4$. If V is made very negative with respect to V_p , then the electron current would be completely suppressed. The saturation current density for negative V is then just $en_i \bar{c}_i/4$.

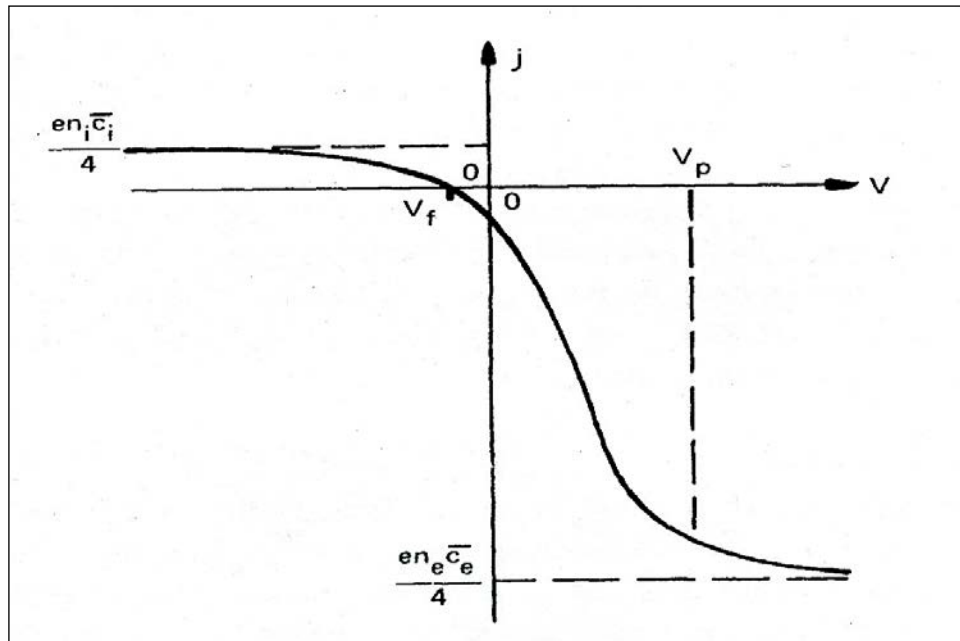


Figure 3.6. Current density-voltage characteristics of a probe. The figure is taken from Chapman, B.N., Glow Discharge Processes [2]

The electron current density j_e to the probe at voltage V should follow the form

$$j_e = \frac{en_e \bar{c}_e}{4} \exp\left(-\frac{e(V_p - V_f)}{kT_e}\right) \quad (3.16)$$

and hence

$$\ln j_e = \ln \frac{en_e \bar{c}_e}{4} - \frac{e(V_p - V_f)}{kT_e} \quad (3.17)$$

This expression is derived on the assumption that the electrons have a Maxwellian energy distribution and it predicts that $\ln j_e$ is linearly dependent on $(V_p - V)$. This prediction is substantiated by experimental results as shown Figure 3.7.

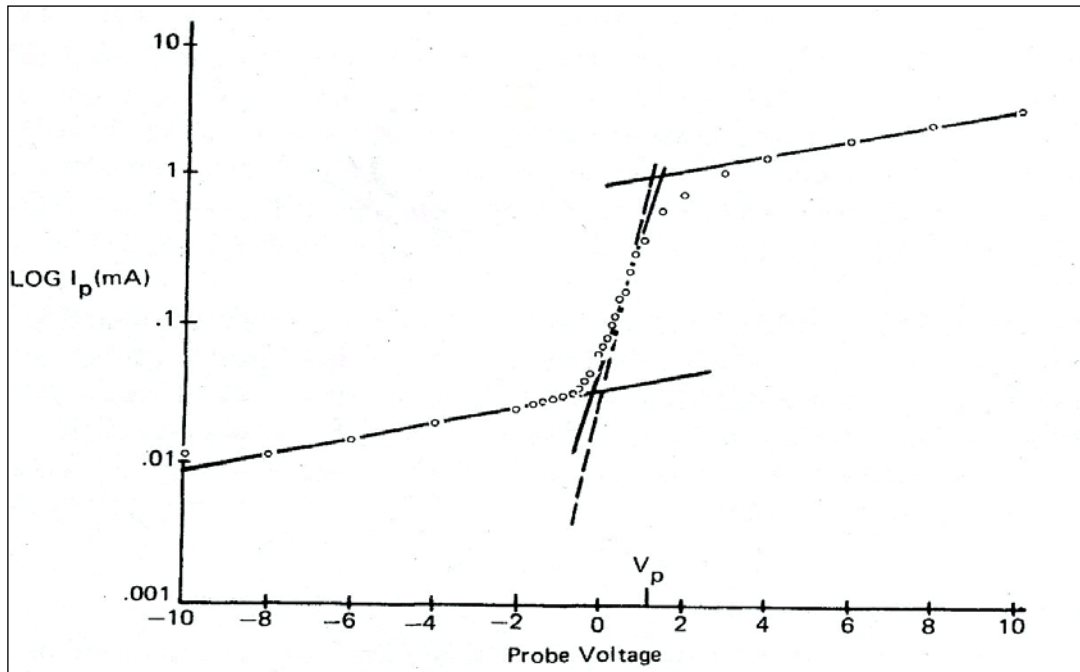


Figure 3.7. Typical probe characteristics showing a quasi-linear region where $\log \propto (V - V_s)$ [22]. Tantalum target, 1000 cm^2 . Argon discharge at 10 mTorr , 3 keV and 59 mA . The figure is taken from Chapman, B.N., *Glow Discharge Processes* [2]

The net current density to the probe, for $V < V_p$, is just the sum of j_i and j_e

$$j = \frac{en_i \bar{c}_i}{4} - \frac{en_e \bar{c}_e}{4} \exp\left(-\frac{e(V_p - V)}{kT_e}\right) \quad (3.18)$$

By a similar argument, one would expect for $V > V_p$ that

$$j = \frac{en_i \bar{c}_i}{4} \exp\left(-\frac{e(V - V_p)}{kT_i}\right) - \frac{en_e \bar{c}_e}{4} \quad (3.19)$$

and also, since $T_i \ll T_e$, that the ion current term would rapidly go to zero as soon as V exceeds V_p , leaving the electron saturation current and fairly well-defined V_p at the knee of the curve.

In principle, this probe technique, which was introduced by Irving Langmuir and colleagues in the 20's [19-21] and carries his name, should be able to give us quite simply

all of the parameters of the plasma that we need to know- electron and ion temperatures, plasma density and plasma potential.

3.2.1. Practical Complications

Unfortunately, the situation with real probe measurement is much more complex, for a variety of reasons. The effective current-collecting area of the probe is not its geometric surface area, but rather the area of the interface between the plasma and the sheath around the probe in Figure 3.8; and the thickness of the sheath, for a given plasma, is a function of the probe potential. This would not matter for a plane probe except that such a probe has ends where the problem arises again; and the relative contribution of the problem is increased because of the requirement that the probe be small, so that the probe current does not constitute a significant drain on the plasma. With a cylindrical probe, the varying sheath thickness is an even larger effect.

Two more complications are associated with additional charge generation. Secondary electrons may be generated at the probe due directly to the impact of ions and electrons and photons or the heating effects caused by such impact, giving rise to additional current flow ; electron impact ionization may occur in the sheath, again enhancing current flow.

Yet one more problem concerns the tendency of charged particles to take up orbital paths around the probe, further influencing the probe characteristics. Even our assumption that the ion current density at the edge of the sheath is equal to the random density $en_i c_i/4$, turns out to be incorrect. And in the glow discharges used in sputtering and plasma etching, there are additional difficulties due to directed high energy electrons which flow through the plasma.

All of these effects, and others that exist, add considerable complexity to proper interpretation of probe data [26-32].

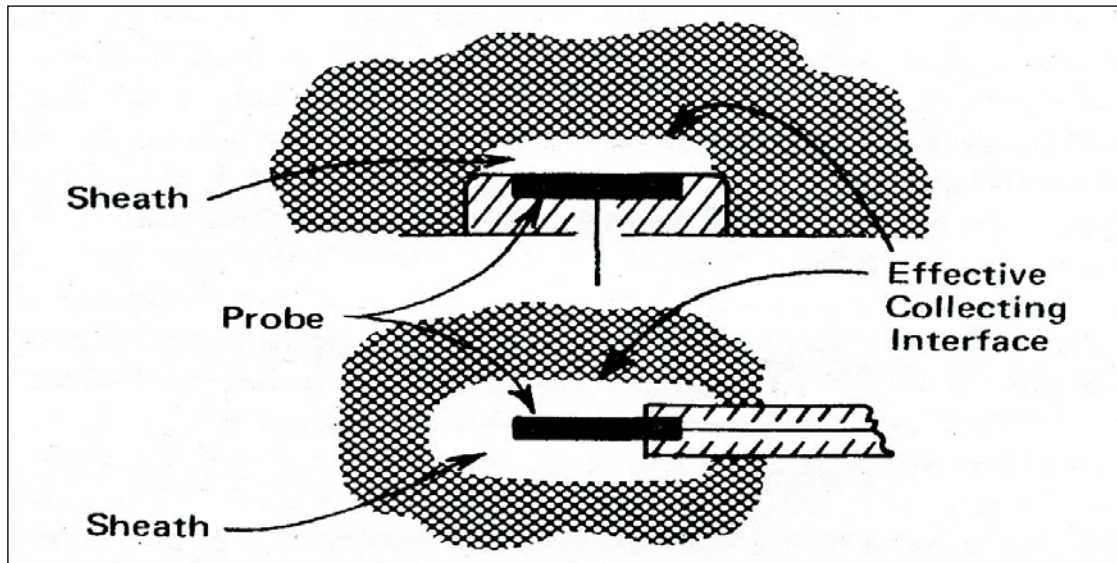


Figure 3.8. Effective current-collecting areas of probes. The figure is taken from Chapman, B.N., *Glow Discharge Processes* [2]

3.2.2. Positively Biased Probes

Another probe effect is quite difficult to deal with: as soon as the probe potential approaches the plasma potential, the electron current density to the probe should approach the saturation value, $en_e c_e/4$. However, even with a tiny probe, the actual current drain can easily become a serious drain on the plasma, causing a significant perturbation, at least for glow discharge processes, which are of rather low density. This current drain can be limited by minimizing the size of the probe, but the following example shows that a very small probe is required. Use the typical plasma parameters shown in Figure 3.1 and a total current of 10mA . Let us estimate a tolerable electron current drain of 1mA . Since the random electron current density is $38\text{mA}/\text{cm}^2$ (Plasma Potential), 1mA would be drawn by a collection area of $2.6 \times 10^{-2}\text{cm}^2$. Imagine a thin cylindrical wire probe 0.25cm in length; such a collection area would correspond to a cylinder radius of $166\text{ }\mu\text{m}$. But this radius corresponds to the sum of the probe and sheath radii Figure 3.8 and the sheath itself is going to: 1 Debye length, which alone is $105\text{ }\mu\text{m}$ for our example.

The effect of attempting to draw too much electron current from the plasma is illustrated in Figure 3.9 where the probe circuit of Figure 3.5 is redrawn along with the discharge circuit.

The electron current to the probe is in addition to the electron current to the anode. So either the ion current to the cathode must increase or the electron current to the anode must decrease. Under normal circumstances where the probe circuit supplies very little power to the discharge, the latter dominates. A decrease in the electron current to the cathode is accomplished by an increase in the plasma potential, causing more electron retardation in the anode sheath. One arrives at the same result by arguing that the probe starts to drain the plasma of electrons, leaving it space charge positive so that the plasma potential has to rise; or by arguing that the probe becomes the new anode as soon as its potential exceeds that of the original anode and that the plasma potential is determined by the anode potential and the need to maintain current continuity in the circuit. Coburn and Kay [23] have encountered just this difficulty of not being able to find a small enough probe for sputtering discharges, and, using an independent technique to determine plasma potential based on measuring the energy distribution of ions accelerated across a sheath, have found that application of positive probe voltages serves only to increase the plasma potential.

The conclusion that, at least in the rather tenuous discharge of sputtering and plasma etching, the plasma potential will be the most positive potential in the system. This becomes increasingly true with increasing size of the perturbing electrode.

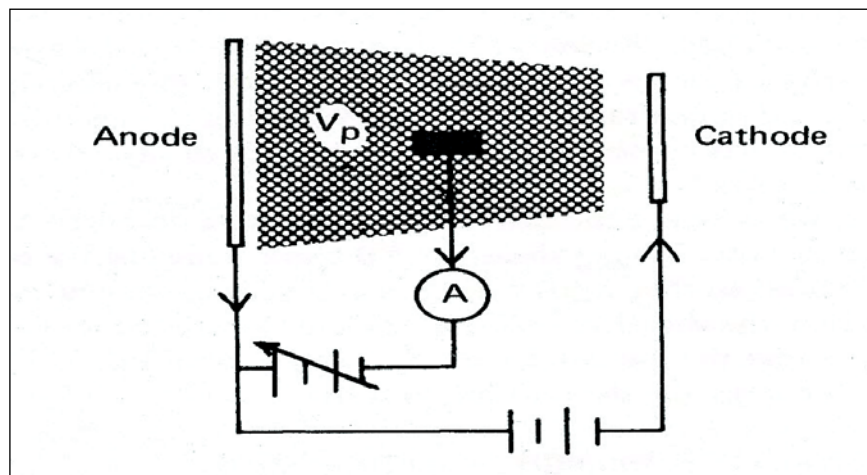


Figure 3.9. Schematic of probe and discharge circuits. The figure is taken from Chapman, B.N., Glow Discharge Processes [2]

3.3 SHEATH FORMATION AND BOHM CRITERION

In the section plasma potential, we calculated the random ion current density $n_i c_i / 4$ which flows in the plasma and found that it had a value of $2 \mu A / cm^2$ for a typical plasma of density $10^{10} / cm^3$ and ion temperature $500 K$. The ion current density to any object more negative than the plasma potential should be equal to the random ion current density. The substrate was electrically floating so that the net current flow was zero. However, it is simple matter to extend the arguments given there to include the case where there is net ion current to the object, and one would still expect to find a current density of $21 \mu A / cm^2$. But if we measure the current density at the target in a *DC* sputtering glow discharge, we find that the current density is larger, of the order of a few tenths of a milliamp per square centimeter. Although we shall learn in the next chapter that some of this latter current is due to the emission of electrons from the target, there is apparently a discrepancy in these two values of current density. Although the ion temperature which we used to derive \bar{c}_i was only an estimate, this estimate can not be far out and anyway \bar{c}_i varies as the square root of the ion temperature which is rather a weak dependence. So the reason for the discrepancy must lie elsewhere.

The problem turns out to be due to an oversimplification of the model for the sheath. We had assumed that the sheath terminated at the plane where the ion and electron densities became equal, to become an undisturbed plasma again in Figure 3.4. In fact, between these two regions there is a quasi-neutral transition region of low electric field as seen Figure 3.10, and the effect of this region is to increase the velocity of ions entering the sheath proper. The existence of this velocity change was demonstrated by Bohm [24] and the resulting criterion for sheath formation has come to be known as the Bohm sheath criterion, and is demonstrated as follows:

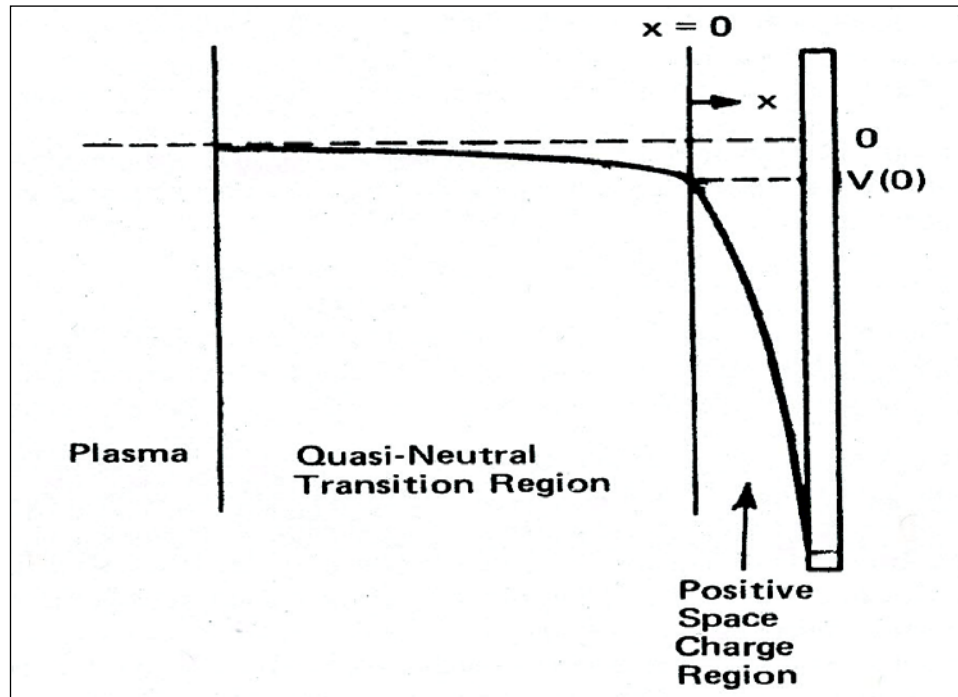


Figure 3.10. Potential variation near a negative electrode. Density $n_i(x)$ and potential $V(x)$ at $x \geq 0$. The figure is taken from Chapman, B.N., Glow Discharge Processes [2]

In Figure 3.10, we assume a monotonically decreasing potential $V(x)$ as ions traverse the positive space charge sheath; $x = 0$ corresponds to the boundary between the two regions so that $n_i(0) = n_e(0)$, i.e. space charge neutrality at $x = 0$. We also assume that the sheath is collisionless and the consequent absence of ionization ensures that the ion current $en_i(x)u(x)$ is constant.

Conservation of energy for the ions requires that

$$\frac{1}{2} m_i u(x)^2 = \frac{1}{2} m_i u(0)^2 - e[V(x) - V(0)] \quad (3.20)$$

Therefore,

$$u(x) = \left(u(0)^2 - \frac{2e[V(x) - V(0)]}{m_i} \right)^{\frac{1}{2}} \quad (3.21)$$

and

$$n_i(x) = \frac{n_i(0)u(0)}{u(x)} = n_i(0) \left(1 - \frac{2e[V(x)-V(0)]}{m_i[u(0)]^2}\right)^{\frac{1}{2}} \quad (3.22)$$

By the Boltzmann relation for the electrons

$$n_e(x) = n_e(0) \left(\frac{e[V(x)-V(0)]}{kT_e}\right) \quad (3.23)$$

Poissons's equation is then

$$\begin{aligned} \frac{d^2\phi}{dx^2} &= \frac{e}{\epsilon_0} (n_e(x) - n_i(x)) \\ &= en_e(0) \left(\exp\left(\frac{e[V(x)-V(0)]}{kT_e}\right) - \left(1 - \frac{2e[V(x)-V(0)]}{m_i[u(0)]^2}\right)^{\frac{1}{2}} \right) \end{aligned} \quad (3.24)$$

But if this is to be a positive space charge sheath, then d^2V/dx^2 must be negative for all $x > 0$ (and zero for $x = 0$) i.e.

$$\left(1 - \frac{2e[V(x)-V(0)]}{m_i[u(0)]^2}\right)^{-\frac{1}{2}} > \exp\left(\frac{e[V(x)-V(0)]}{kT_e}\right) \quad (3.25)$$

Squaring and inverting, then

$$\exp\left(-\frac{2e[V(x)-V(0)]}{kT_e}\right) > 1 - \frac{2e[V(x)-V(0)]}{m_i[u(0)]^2} \quad (3.26)$$

We now restrict our attention to the beginning of the space charge sheath where $V(x) - V(0)$ is very small compared to kT_e so that we can expand and approximate the exponential ($e^{\pm x} \approx 1 \pm x$ for $x \ll 1$), thus

$$1 - \frac{2e[V(x)-V(0)]}{kT_e} > 1 - \frac{2e[V(x)-V(0)]}{m_i[u(0)]^2} \quad (3.27)$$

i.e.

$$u(0) > \left(\frac{kT_e}{m_i}\right)^{\frac{1}{2}} \quad (3.28)$$

This says that the ion velocity on entering the sheath must be greater than $(kT_e/m_i)^{1/2}$, i.e. is determined by the electron temperature, which is a rather peculiar result and demonstrates how the ion and electron motions are coupled. Chen [25] demonstrates Figure 3.11 that the physical significance of the criterion is that the acceleration of ions in the sheath and repulsion of electrons there, both of which decrease the relevant particle volume densities, must be such that the ion density decreases rapidly than the electron density across the sheath. This is equivalent to the requirement that dV^2/dx^2 is negative, and it is clear from Figure 3.11 that this requirement is most stringent at the beginning of the sheath where $V(x) - V(0)$ is very small, as we assumed.

How do the ions acquire this velocity? There must be an electric field across the transition region so as to give the ions a directed velocity of $u(0)$ towards the electrode. If we assume that the ion temperature is negligibly small so that the random motion of the ions can be neglected, then since the potential at the boundary is $V(0)$ with respect to the plasma,

$$\frac{1}{2}m_i u(0)^2 = eV(0) \quad (3.29)$$

so

$$V(0) = \frac{m_i u(0)^2}{2e} = \frac{m_i kT_e}{2em_i} = \frac{kT_e}{2e} \quad (3.30)$$

The existence of a field in the transition region does not contradict our earlier claim that the plasma is equi-potential, since that claim was qualified then to the extent that voltages of the order of kT_e/e could *leak* into the plasma.

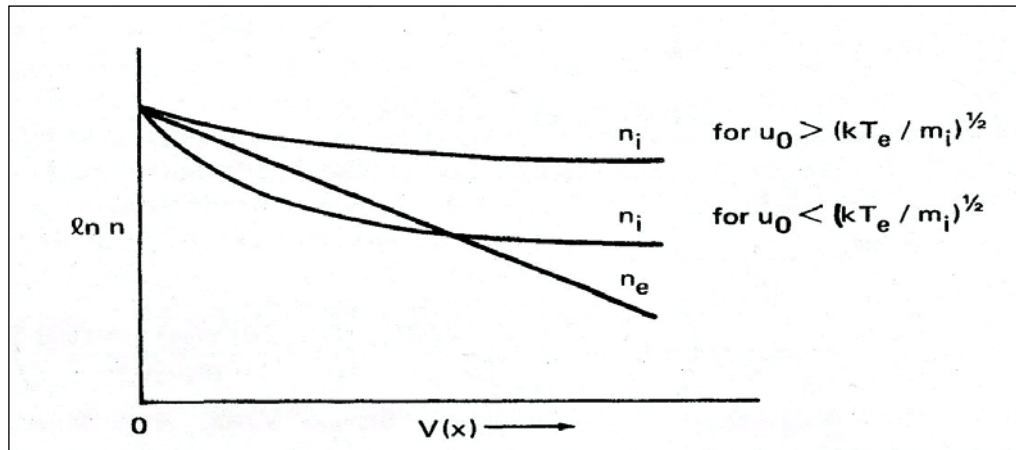


Figure 3.11. Variation of ion and electron density with potential $V(x)$ in a sheath for $u_0 > (kT_e/m_i)^{1/2}$ and $u_0 < (kT_e/m_i)^{1/2}$. The figure is taken from Chapman, B.N., Glow Discharge Processes [2]

We can pursue the exercise further to calculate the ion flux at the sheath boundary. Since the potential there is $V(0)$ with respect to the plasma in which the electron density is n_e , then using the Boltzmann relation again,

$$n_e(0) = n_e \exp\left(-\frac{V(0)}{kT_e}\right) = n_e \exp\left(-\frac{1}{2}\right) = 0.6n_e \quad (3.30)$$

and using $n_e(0) = n_i(0)$, the ion flux is given by

$$n_i(0)u(0) = 0.6n_e \left(\frac{kT_e}{m_i}\right)^{1/2} \quad (3.31)$$

Substituting in the values from Table 3.1 again, we obtain an ion current density of 0.2 mA/cm^2 , which is more like reality. However, this derivation is still not quite realistic since it assumes that the ion temperature is zero, which is never so; and that there are no collisions in the sheath, which is not true for the sheaths that form in front of low voltage anodes and probes. We also know that the cathode current depends on the cathode voltage in practice, and the ion current expression derived above does not explicitly include the electrode voltage except to the extent that the electrode voltage does control the electron temperature and plasma density.

The effect of the Bohm criterion is to increase the ion flux to any object negatively biased with respect to the plasma. In particular it will change the ion flux to a floating substrate. We had calculated the floating and apparently we must now change this to allow for this changed ion flux.

Using a similar derivation to before, the criterion for net zero current becomes

$$\left(n_e \exp\left(-\frac{e(V_p - V_f)}{kT_e}\right) \right) \frac{c_e}{4} = n_i 0.6 \left(\frac{kT_e}{m_i} \right)^{\frac{1}{2}} \quad (3.32)$$

Hence

$$V_p - V_f = -\frac{kT_e}{e} \ln 2.4 \left(\frac{kT_e}{m_i} \right)^{\frac{1}{2}} \left(\frac{\pi m_e}{8kT_e} \right)^{\frac{1}{2}} = -\frac{kT_e}{e} \ln \left(\frac{m_i}{2.3m_e} \right) \quad (3.33)$$

In our example it shown Table 3.1, $V_p - V_f$ should have a value of 10.4 V compared with 15 V. The larger ion flux requires a larger electron flux for current neutrality, and so a smaller electron retarding potential. The logarithmic dependence minimizes the change in potential due to the increased ion flux.

4. THE ELECTRICAL PROBE METHOD

4.1. A TWO-ELECTRODE SYSTEM

Although the experimental determination of the probe characteristics is comparatively simple this is unfortunately not true of the theoretical analysis. This has proved to be extremely complicated, in general, there being no one universal method of interpretation [28]. The reason for difficulty stems from the application of the method to diagnosis of so many different types of plasmas, ranging from partially ionized gases at very low pressures to highly ionized gases at high pressures.

When a potential difference is applied between two electrodes immersed in a partially ionized but macroscopically neutral gas, the positive ions will be attracted towards the negative electrode and the electrons towards the positive electrode. That is, the applied electric field attempts to destroy the neutrality of the plasma by separating the positive and negative charge carriers. This separation is immediately opposed by the high microscopic electric fields set up between the charge carriers of opposite sign once they have been displaced from their previous position of macroscopic neutrality. However, charge separation can occur in the immediate neighbourhood of the two electrodes as a result of carrier absorption. The regions, adjacent to the two electrodes, in which plasma neutrality no longer exists are known as the 'sheath regions' and it is here that most of the applied potential difference is developed.

It should be appreciated that the applied potential difference must never be so large that ionization can occur in the sheath regions. A situation that allows the development of a discharge between the two electrodes should never be permitted, since conditions in the plasma are then being disturbed. The electrodes should not, therefore, emit electrons either thermodynamically or by any secondary process. In other words, the ions and electrons in the space between the electrodes should solely result from processes that are completely independent of the two-electrode system being discussed. The only part the plasma plays is to complete the electrical circuit between the two electrodes. As it is hoped to gain some information about the plasma from measurements of the current flowing in the electrode

circuit, the electrode current must never be so large as to drain the plasma to any appreciable extent.

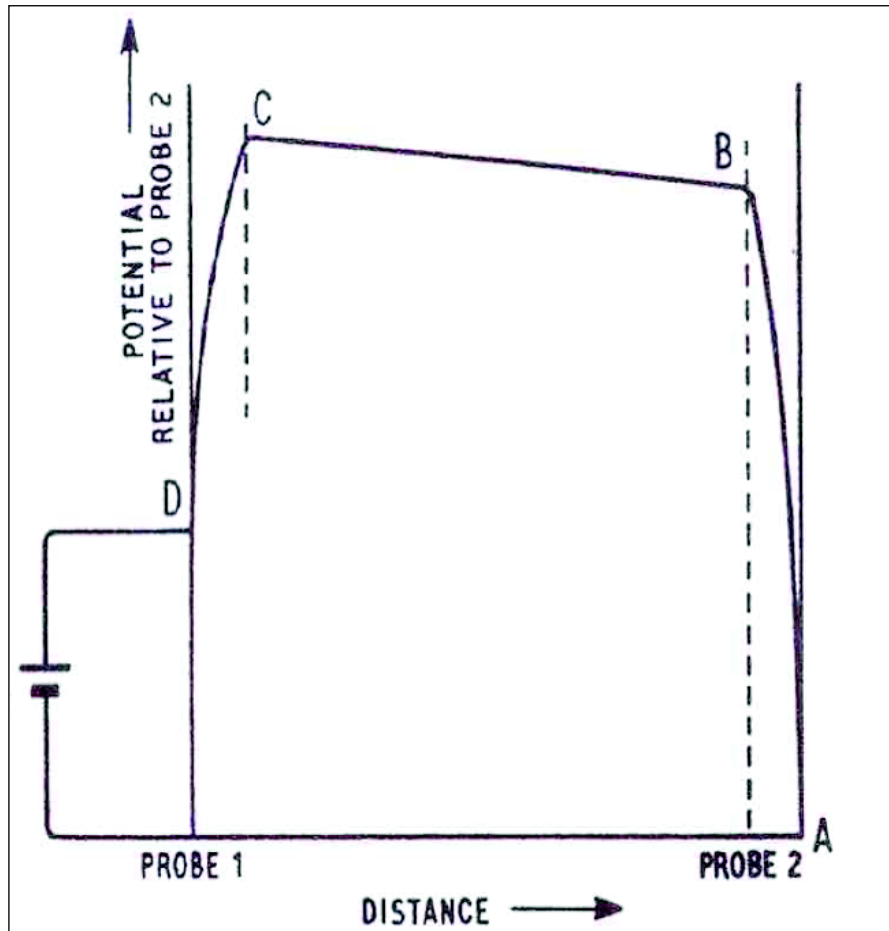


Figure 4.1. Two-electrode circuit. The figure is taken from Swift, J.D. and Schwar, M.J.R., Electrical Probes for Plasma Diagnostics [28]

Figure 4.1 shows the potential distribution in a two-electrode system. AB and CD represent the potential drops across the sheath regions and BC the potential drop across the neutral plasma. It is considered at this stage a general system where the electrodes can be positive or negative with respect to the surrounding plasma, but the latter situation is normal.

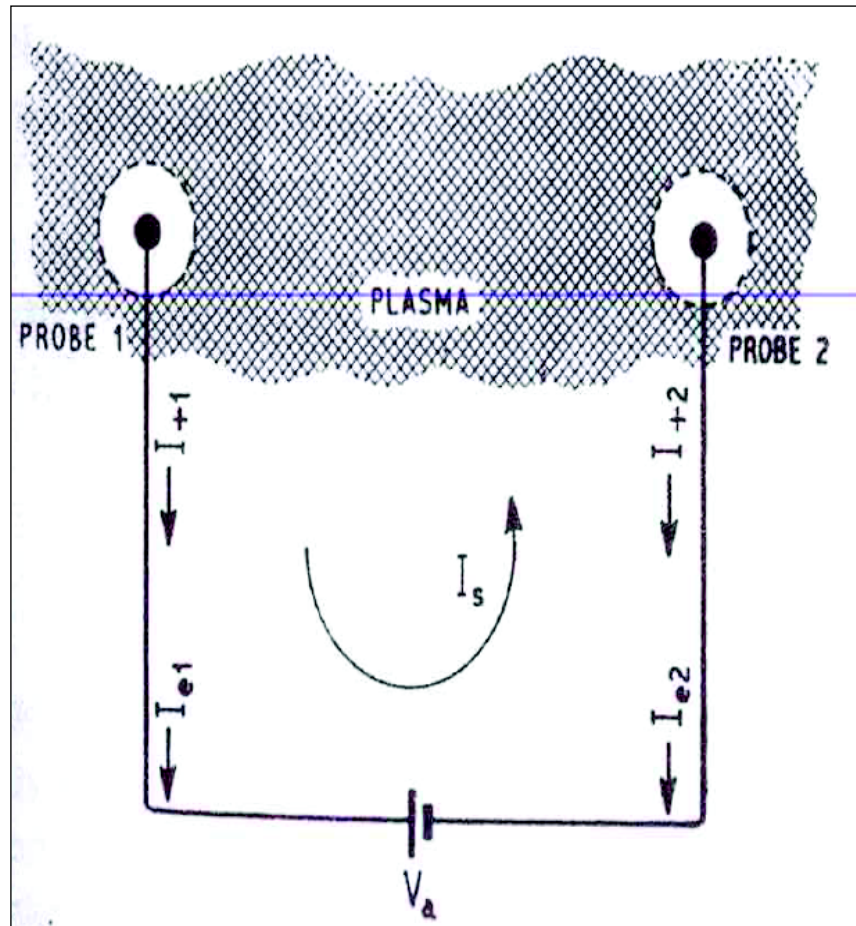


Figure 4.2. Potential distribution in a two-electrode system. The figure is taken from Swift, J.D. and Schwar, M.J.R., *Electrical Probes for Plasma Diagnostics* [28]

The potential drop across BC is generally the result of spatial variations in plasma properties rather than the potential drop system. V_{BC} , therefore, is generally independent of the current flowing in the two electrode system, and thus of externally applied potential difference V_a .

The potential drops across AB and CD will vary with V_a , their magnitudes being controlled by the following two requirements. Examination of Figure 4.1 clearly shows

$$V_{AB} + V_{BC} = V_{CD} + V_a \quad (4.1)$$

The second requirement is that of current continuity in the circuit of the two-electrode system. If I_s is the circuit current, and I_{e1} and I_{+1} are the electron and positive ion

currents flowing from the plasma to probe 1 , and I_{e_2} and I_{+2} are the corresponding currents to probe 2 we have,

$$I_s = I_{e_1} + I_{+1} \quad (4.2)$$

$$I_s = -(I_{e_2} + I_{+2}) \quad (4.3)$$

where the positive directions of the various current components are shown as in Figure 4.1.

Combining Equations 4.2 and 4.3

$$I_{e_1} + I_{e_2} = -(I_{+1} + I_{+2}) \quad (4.4)$$

As I_e and I_+ are functions of the probe to plasma potential V_{AB} and V_{CD} adjust themselves so as to satisfy Equations 4.1 and 4.4.

When no potential difference exists between the electrode and plasma, the carrier current reaching the electrode is equal to the random current density multiplied by the electrode's surface area.

$$I = A_p \frac{N_c \bar{c}}{K} q \quad (4.5)$$

Where N_c , \bar{c} and q are the carrier density, mean speed and charge, respectively. K is a numerical factor. However, that for a spherical probe the value of K depends on the ratio of the carrier free path to the electrode radius, l/rP , and always lies between 0.5 and 1. When $l/rP \gg 1$, K approaches 14 and Equation 4.5 reduces to the expected result. When $l/rP \ll 1$, K approaches 0.5. If the polarity of the electrode to plasma potential is such that carriers are attracted the electrode current is greater than that given by Equation 4.5. The electrode current increases slowly with an increase in the attracting potential. If the polarity of electrode to plasma potential is such that carriers are repelled, however, the electrode current is less than that given by Equation 4.5. The electrode current then decreases rapidly as the retarding electrode to plasma potential increases.

The ratio of the random electron to random positive ion current density is given by following equation when the electron and positive ion energy distributions are both Maxwellian, corresponding to effective temperatures T_e and T_+ respectively,

$$\frac{i_e}{i_+} = \frac{K_+ \bar{c}_e}{K_e \bar{c}_+} = \frac{K_+}{K_e} \left(\frac{T_e}{m_e} \cdot \frac{m_+}{T_+} \right)^{\frac{1}{2}} \quad (4.6)$$

It should be noted that $K_e \neq K_+$ in general since the mean free paths of electrons and ions are not normally the same. In the case of electrons and positive ions of hydrogen H_+ at the same temperature and when $K_e = K_+$, $i_e/i_+ \cong 43$. In an *active* plasma i_e/i_+ will normally be greater than this, since $T_e > T_+$ in general. In order satisfy Equation 4.4 when the two electrodes are of comparable surface area, the potential drops across both the sheath regions must be such as to repel the arrival of electrons. Thus both electrodes are normally negative with respect to the surrounding plasma, as shown in Figure 4.1, irrespective of the value of the applied potential difference V_a .

4.2. THE DOUBLE PROBE SYSTEM

When the two electrodes are of comparable surface area and are both at a negative potential with respect to the plasma for all values of V_a the system is called a *double probe system*. The variation of circuit current, I_s , with V_a is known as the *double probe characteristic* and analysis of this characteristic.

One problem in the interpretation of a double probe characteristic is that V_{AB} and V_{CD} both vary with V_a , and it is extremely difficult, in general, to relate the observed variation of I_s with V_a to the variation of I_s with either V_{AB} or V_{CD} . This is necessary, however, because all theoretical analyses describing the flow of carriers to a bias probe express the probe current in terms of the probe to plasma potential V_{AB} , V_{CD} . Figure 4.3 shows a typical double probe characteristic.

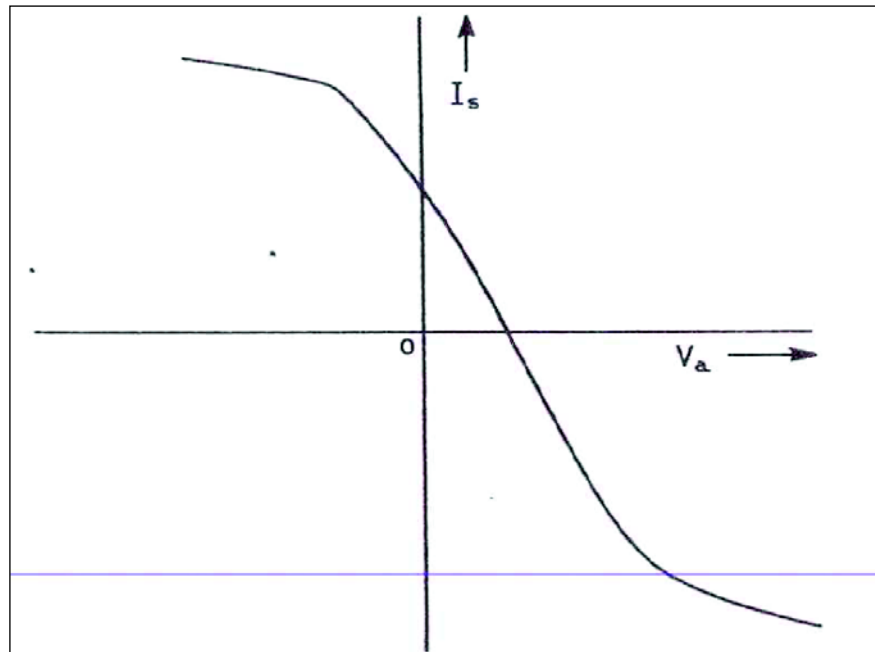


Figure 4.3. Typical double-probe characteristics. The figure is taken from Swift, J.D. and Schwar, M.J.R., *Electrical Probes for Plasma Diagnostics* [28]

An advantage of a double probe system is that the maximum current drain from the plasma is readily limited to any desired value by simply limiting the size of the two probes. This maximum current is practically independent of the polarity or magnitude of V_a and is given by $\sum I_+$ the sum of the saturation positive ion currents to the two electrodes Equation 4.4.

4.3. THE SINGLE PROBE SYSTEM

A simpler system would be one in which the electrode to plasma potential for the second electrode can be varied without affecting the electrode to plasma potential of the first electrode. In terms of Figure 4.1 this is equivalent to varying V_{CD} as V_a varies without affecting V_{AB} and V_{BC} . Rewriting Equation 4.1

$$V_{CD} + V_a = V_0 \quad (4.7)$$

where V_0 is a constant independent of V_a . V_0 is the potential of C relative to A and is known as the *plasma potential*.

We must now examine the necessary conditions for the potential of C relative to A to remain constant and independent of V_a . In other words, no part of the two-electrode circuit is connected to a point of fixed potential with respect to the plasma. One way in which the potential at C (i.e. relative to A) can be kept reasonably constant is to make the second electrode very much larger than the first. In this case the larger electrode is known as the *reference electrode* and the smaller electrode as the *single probe* or simply *probe*, and is usually of spherical, cylindrical or planar geometry.

If the reference electrode area A_2 is sufficiently large compared with A_1 , I_{+2} can be made to exceed I_{e_1} even when the probe is at plasma potential ($V_{CD} = 0$ in Figure 4.1). It is then possible to vary the probe potential, by varying V_a , without appreciably affecting the reference electrode to plasma potential. This is because Equation 4.4 is now approximately satisfied with $-I_{+2} = I_{e_2}$, i.e. with V_{AB} fixed, irrespective of the values of I_+ and I_e . It is clear from Equation 4.6 that the reference electrode is strongly negative with respect to the plasma.

An optimum area ratio for smaller electrode to act as a single probe. Referring to Figure 4.1 let us consider what happens as the inter-electrode potential, V_a , is varied. As V_a is decreased the probe to plasma potential becomes more negative and I_{e_1} is greatly reduced while I_{+1} is very slightly increased. In order that Equation 4.4 should still be satisfied these changes must be accompanied by an increase in I_{e_2} and/or a decrease in I_{+2} . Because of the very large area ratio a change in I_{e_2} comparable to the change in I_{e_1} can be achieved by a very small reduction in the reference electrode to plasma potential.

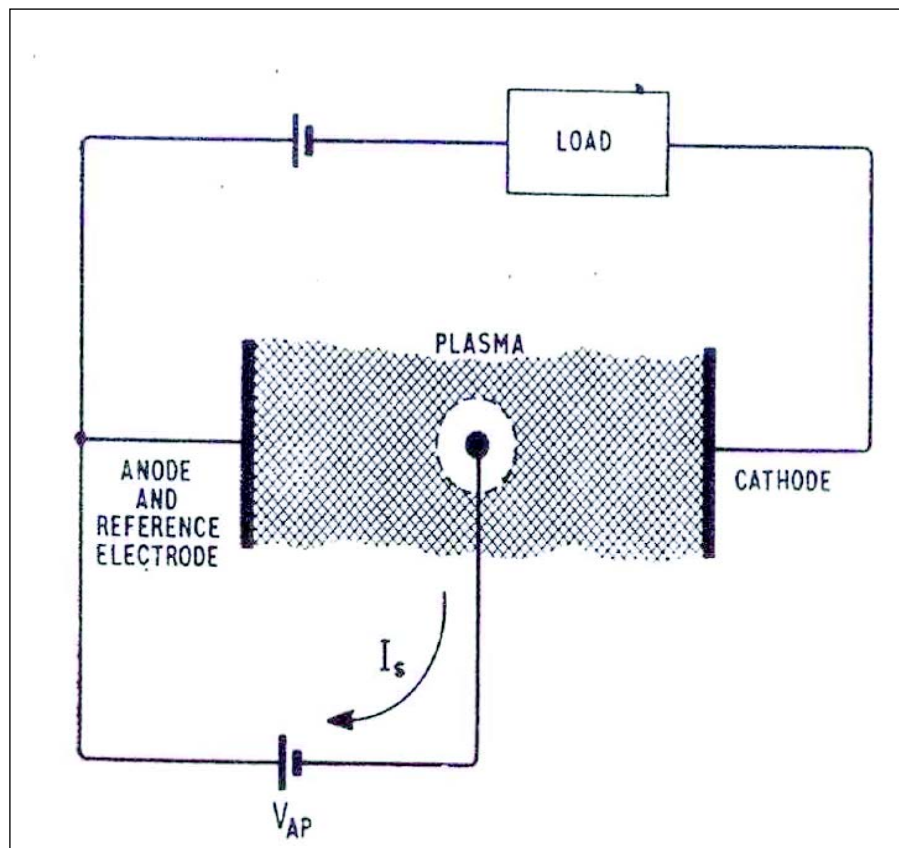


Figure 4.4. Single probe circuit. The figure is taken from Swift, J.D. and Schwar, M.J.R.,
Electrical Probes for Plasma Diagnostics[28]

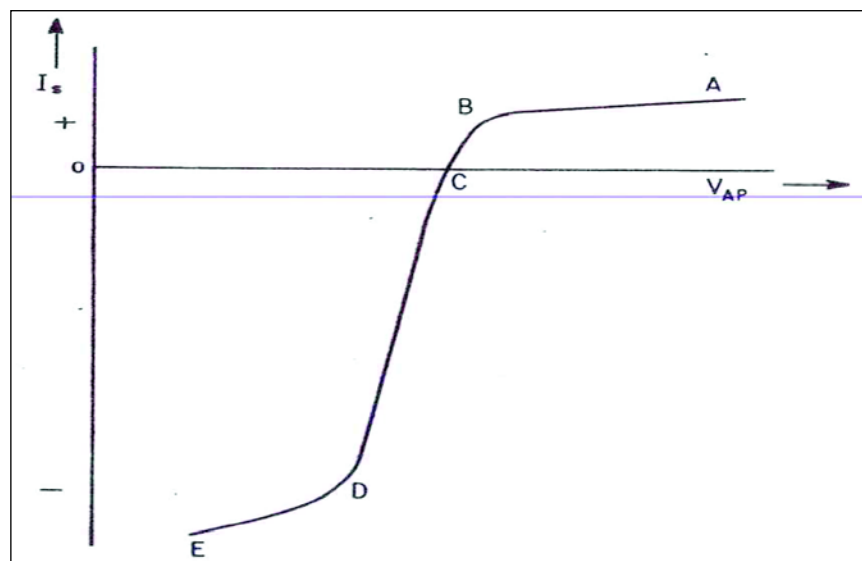


Figure 4.5. Single probe characteristics. The figure is taken from Swift, J.D. and Schwar, M.J.R.,
Electrical Probes for Plasma Diagnostics

Likewise V_a can be increased so as to drive the probe positive with respect to the plasma. In this region I_{e_1} varies only slowly with the probe to plasma potential so changes in V_a are accompanied by even smaller changes in the reference electrode to plasma potential than were present when the probe was being operated in the electron retarding region.

Another way of ensuring that the potential at C remains constant and independent of V_a is to make the reference electrode an integral part of the plasma circuit, e.g. make it either the anode or cathode of a discharge circuit. In this case the circuit will be as shown in Figure 4.3 where V_{AP} , the potential drop from anode to probe, corresponds to $-V_a$ of the previous discussion. As before, potential drops exist across the sheath regions that form next to the electrodes. In this case, however, the potential drops next to the cathode and anode depend only on the conditions that exist in the plasma and are independent of the probe current, provided the probe does not disturb the discharge conditions. This will normally be the case if the probe current I_s is negligible in comparison with the discharge current I . In this circuit the potential at C in Figure 4.1 remains constant and independent of V_{AP} . Figure 4.5 shows a typical single probe characteristic.

4.4. ELEMENTARY PROBE THEORY FOR LOW PRESSURE PLASMAS

The theory of the flow of charge carriers to an electrical probe can be extremely complex. The numerous analyses presented arise from the need to apply the electrical probe method to such a wide range of plasmas. Practical plasmas tend to fall into a number of groups, an important one of which is the low pressures below 0.1 Torr .

A simplified introduction to the electrical probe method, as applied to this type of gas discharge, will now be given. The following assumptions are made:

1. Electron and ion concentrations are equal.
2. Electron and ion free paths are much larger than the probe radius.
3. Electron temperature is much larger than the positive ion temperature.
4. Probe radius is much larger than the Debye length.
5. There is a Maxwellian distribution of electron and positive ion velocities.

A low pressure plasma is defined as one in which a probe of sufficiently small diameter produces a negligible disturbance to the carrier concentration and in which the great majority of the applied probe to plasma potential is developed across a region that is much thinner than a carrier mean free path.

It is convenient to consider one particular type of plasma in order that one may better visualize the physical problems involved. We will, therefore assume that the probe is immersed in the positive column of a low pressure glow or arc discharge in which the current is maintained constant.

In the single probe circuit shown in Figure 4.3 the probe, P , may be a spherical, cylindrical or plane electrode whose supports and lead wire are completely insulated from the discharge in which it is immersed. The potential, V_{AP} , between the anode of the discharge and the probe can be varied so that the probe may be either at a higher or a lower potential than the surrounding discharge. The current I_s flowing from the discharge to the probe, which in general consists of an ion current I_+ and an electron current I_e , can be determined for various values of V_{AP} ; this is known as the probe characteristic.

The general form of the probe characteristic is shown in Figure 4.4 and a qualitative interpretation will now be given. When V_{AP} is very large the probe is strongly negative with respect to the discharge and the electric field produced in the space surrounding the probe will prevent even the most energetic electrons in the discharge from reaching it. The probe current I_s is then due entirely to positive ions (section AB in Figure 4.5). This is no longer true when the negative potential is decreased (section BC); the faster electrons are now able to overcome the retarding field so the electron current I_e is no longer negligible and the net probe current I_s is reduced. There is thus a rapid decrease of I_s as V_{AP} is decreased. Eventually I_s passes through zero (C). The potential at which this occurs is usually known as *floating potential* and is the potential that an isolated probe would reach if immersed in the discharge. It is generally several volts below that of the surrounding discharge. This is because the electron diffusion rate greatly exceeds the positive ion diffusion rate. The electron and ion currents to the probe will, therefore, only be equal when the electrons are subject to a retarding potential.

As V_{AP} is decreased still further the probe current, now of opposite sign, increases rapidly owing to the decrease in the field retarding the electrons (section CD). Eventually a point (D) is reached when the probe is at plasma potential. The electrons are now acted on by an accelerating instead of a retarding field and the law governing the increase of electron current changes. This shows itself as a break in the characteristic which occurs at plasma potential (section DE). The sharpness of the break depends markedly on discharge conditions.

4.4.1. Elementary Treatment of Positive Ion Collection

We will now consider the theory of the positive ion part(AB) of the characteristic though a detailed treatment must be deferred. The discussion will be confined to the cases of spherical and cylindrical probes : a plane probe of finite size is rather than unsatisfactory here since the disturbed region surrounding the probe is an ill-defined hemisphere. The first attempt to develop a theory of positive ion collection was made by Langmuir and Mott-Smith [20, 21]. The theory assumed that the region surrounding a negative probe could be divided into two regions:

1. A positive ion space charge sheath into which no electrons can penetrate and
2. The undisturbed plasma in which the ion and electron concentrations are approximately equal and in which there is no penetrating field resulting from the applied probe to plasma potential.

Between the positive ion sheath and undisturbed plasma there is a region (the quasi-neutral region in Figure 4.6) in which the ions and electrons are present in almost equal quantities but in which normal conditions within the plasma have been modified owing to a withdrawal of ions to the probe. Most of the potential drop occurs across the inner sheath and only a relatively small drop occurs across the transitional quasi-neutral region. However, since the mean ion energy in the low pressure discharge is normally much smaller than the mean electron energy, even a weak field penetrating into this region greatly distorts the random thermal motion of the ions. The effect of this is to give the ions at the sheath boundary a directed motion towards the probe; the magnitude of this velocity component is determined primarily by the potential drop across the transition region. Thus

the ions are gathered not by the surface of the sheath but by a larger radius surface lying in the quasi-neutral region.

An estimate of the positive ion current I_+ reaching the probe under these conditions can be made from simple physical considerations. Since the sheath begins when the electron concentration starts to decrease appreciably it is clear that V_s , the potential difference between the sheath edge and the undisturbed plasma, must be just sufficiently large and negative to prevent a significant fraction of the electrons in the discharge from entering the sheath.

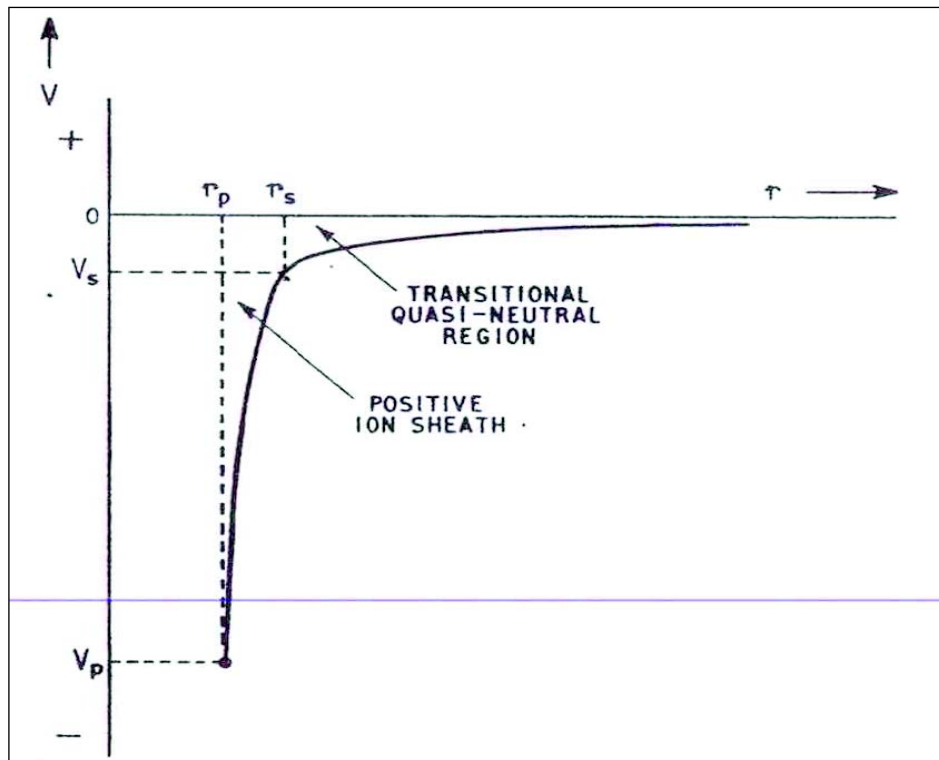


Figure 4.6. Potential distribution in the vicinity of a negative probe. The figure is taken from Swift, J.D. and Schwar, M.J.R., *Electrical Probes for Plasma Diagnostics* [28]

Hence $-eV_s = kT_e/2$, where we assume the electrons to have a Maxwell-Boltzmann distribution corresponding to a temperature T_e . If v_s is the radial velocity of the ions at the sheath boundary we obtain

$$v_s = \sqrt{\frac{-2eV_s}{m_+}} \quad (4.8)$$

where m_+ is the ionic mass and $e < 0$. Now the electron concentration N_e at the sheath boundary is given by

$$N_e = N_\infty \exp\left(+\frac{eV_s}{kT_e}\right) ; V_s < 0 \quad (4.9)$$

where N_∞ is the electron concentration in the undisturbed discharge. Since the ion and electron concentration at the sheath edge are still approximately equal we have for the ion current I_+

$$I_+ = eN_\infty \exp\left(+\frac{eV_s}{kT_e}\right) \sqrt{\frac{-2eV_s}{m_+}} A_s \quad (4.10)$$

where A_s is the area of the sheath surface. Replacing $-eV_s$ by $kT_e/2$ we obtain finally

$$I_+ = \chi N_\infty e \sqrt{\frac{kT_e}{m_+}} A_s \quad (4.11)$$

Where χ is a coefficient of the order of 0.6. χ may differ from this value when T_+ becomes comparable to T_e . In many cases A_s differs little from the area of the probe, although there is some increase in A_s as the probe is made more negative. It should be noted that the factor K appearing in the denominator of Equation 4.5 does not occur in this last equation since Equation 4.11 is applicable only when the effective collecting radius is very much less than the free path of the ions and so $K_+ = 1$.

It is important to note that under these *free fall* conditions the ion current to the probe is determined primarily by the mean electron energy in the discharge rather than the mean ion energy; this is still true even when $T_+/T_e \approx 1$.

4.4.2. Elementary Treatment of Electron Collection

We must next treat the region BD of the characteristic as shown Figure 4.4 where some of the electrons can overcome the retarding potential V_p between probe and discharge. (It is important to note that V_p cannot be measured directly, only V_a is known.)

If we again assume that the electron distribution is Maxwellian and that the gas pressure is sufficiently low for loss of electrons by collision with gas molecules in crossing the sheath to be unimportant, the electron current I_e flowing to a probe of any non-concave shape is given by

$$I = I_0 \exp\left(+\frac{eV_p}{kT_e}\right) ; V_p < 0 \quad (4.12)$$

where I_0 is the electron current reaching the probe when the latter is at plasma potential ($V_p = 0$). This is given by

$$I_0 = -\frac{1}{4} N_\infty \bar{c}_e A_p = -N_\infty e A_p \sqrt{\frac{kT_e}{2\pi m_e}} \quad (4.13)$$

where A_p is the surface area of the probe and \bar{c}_e is the mean thermal speed of an electron in the discharge.

If V_{A0} is the potential difference between the discharge in the vicinity of the probe and the anode then

$$V_a = V_{A0} + V_p ; V_p < 0 \quad (4.14)$$

Equation.4.12 and 4.14 then give

$$\ln(-I_e) = \ln(-I_0) + \frac{e}{kT_e} (V_a - V_{A0}) ; V_a = -V_{Ap} \quad (4.15)$$

A graph of $\ln(-I_e)$ versus V_a is therefore linear, having a slope (e/kT_e) .

4.4.3. Simple Determination of Plasma Parameters

Since the probe current over the greater part of section *BCD* Figure 4.4 is largely due to electrons the slope of the graph of $\ln|I_s|$ versus V_a can be used to obtain the electron temperature T_e in Figure 4.6.

The potential difference between the anode and the discharge in the vicinity of the probe, V_{A0} , is determined from the break in the semilogarithmic characteristic. Knowledge of the current I_0 reaching the probe at plasma potential enables the electron concentration in the undisturbed discharge to be found from Equation 4.13 since T_e is now known. Unfortunately, the break in the characteristic is frequently far from abrupt. The determination of plasma potential, in many cases, corresponds approximately to the start of the derivation of the semilogarithmic characteristic from linearity.

As the probe is biased more and more negative with respect to the plasma the positive ion concentration to the total probe current becomes significant and a correction for this is necessary. This can be done by extrapolating the ion current obtained for a strongly negative probe Figure 4.7. Unfortunately, the law governing such extrapolation is not known accurately in general, and the only satisfactory procedure is to use a screened probe in order to determine the electron and ion contributions separately for each value of V_p .

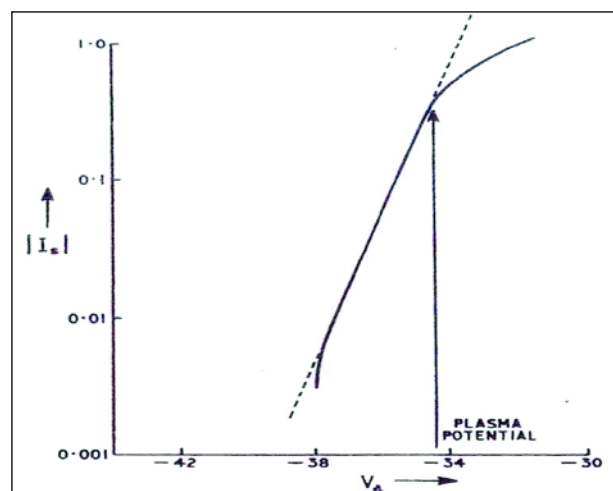


Figure 4.7. Graph of $\ln|I_s|$ versus V_a for deducing the electron temperature. The figure is taken from Swift, J.D. and Schwar, M.J.R., *Electrical Probes for Plasma Diagnostics* [28]

The difference in potential between the probe and the surrounding plasma when the net probe current I_s is zero can be deduced from Equations 4.11 and 4.12. Assuming $A_s = A_p$ we obtain

$$V_f = -\frac{kT_e}{2e} \ln \left[\frac{1}{2\pi\chi^2} \frac{m_+}{m_e} \right] \quad (4.16)$$

where V_f is referred to as floating potential and is generally several volts in magnitude.

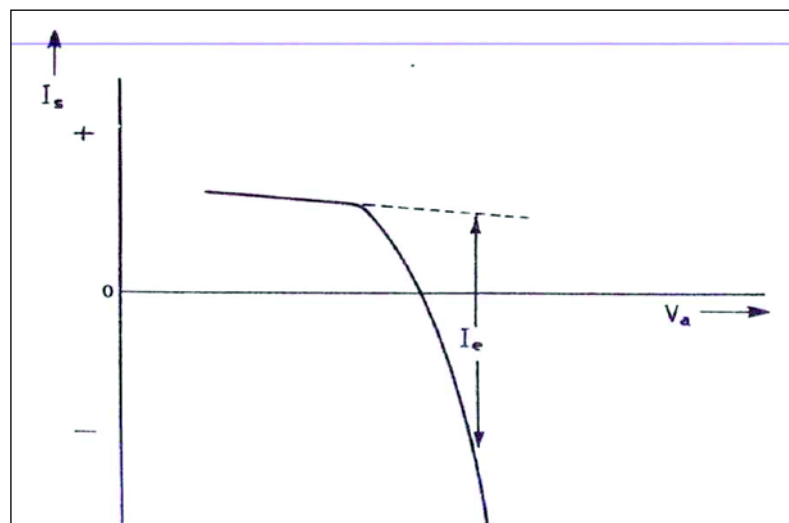


Figure 4.8. Correction for the positive ion contribution to the probe current. The figure is taken from Swift, J.D. and Schwar, M.J.R., *Electrical Probes for Plasma Diagnostics* [28]

5. EXPERIMENTAL RESULTS

Our experimental set up shown in Figure 5.1 includes

1. diffusion pump
2. vacuum chamber
3. mass flow-meter
4. vacuum gauge
5. high voltage source
6. *Ar* gas
7. *DC* power supply with
 - a high resistance of $R = 1k\Omega$
 - a capacitor bank with $C_{eq} = 2\mu F$
 - a diode
 - a transformer

We have designed a *DC* power supply shown in the Figure 5.2.

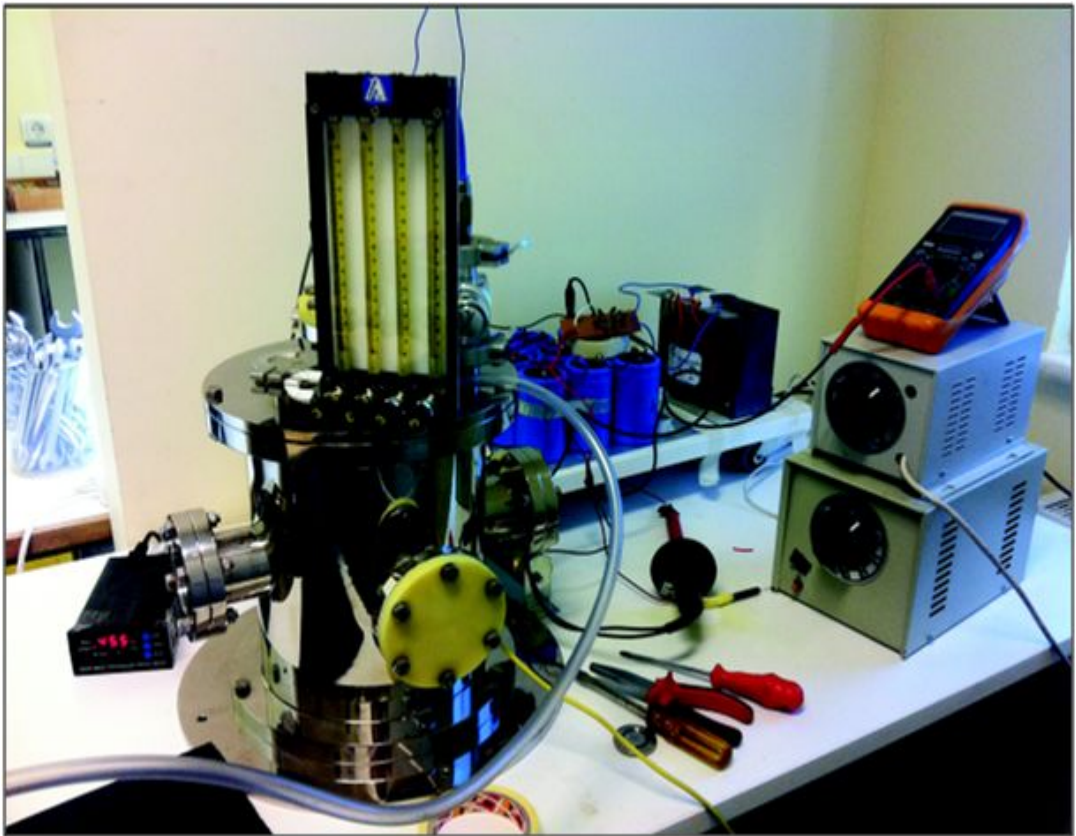


Figure 5.1. Experimental setup

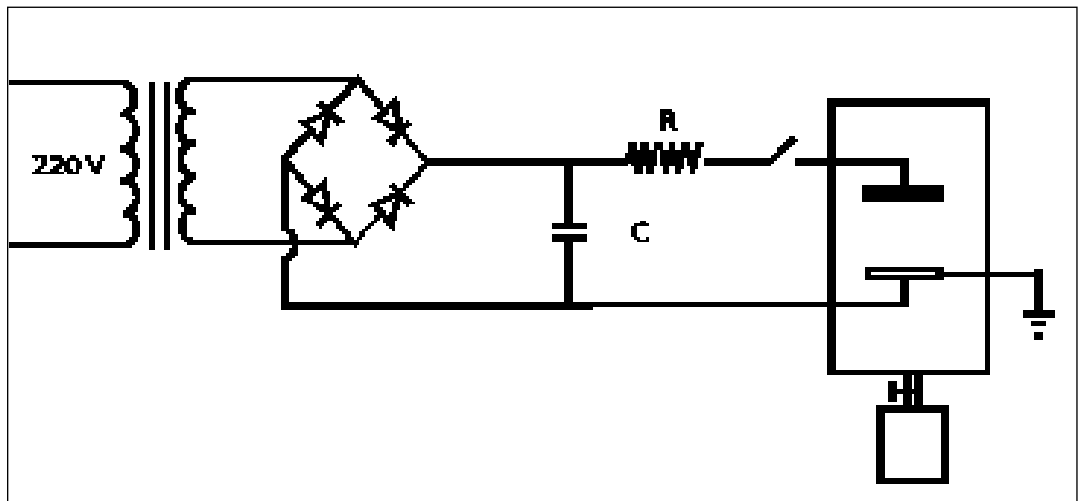


Figure 5.2. The schematic illustration of the design of *DC* power supply



Figure 5.3. Glow discharge

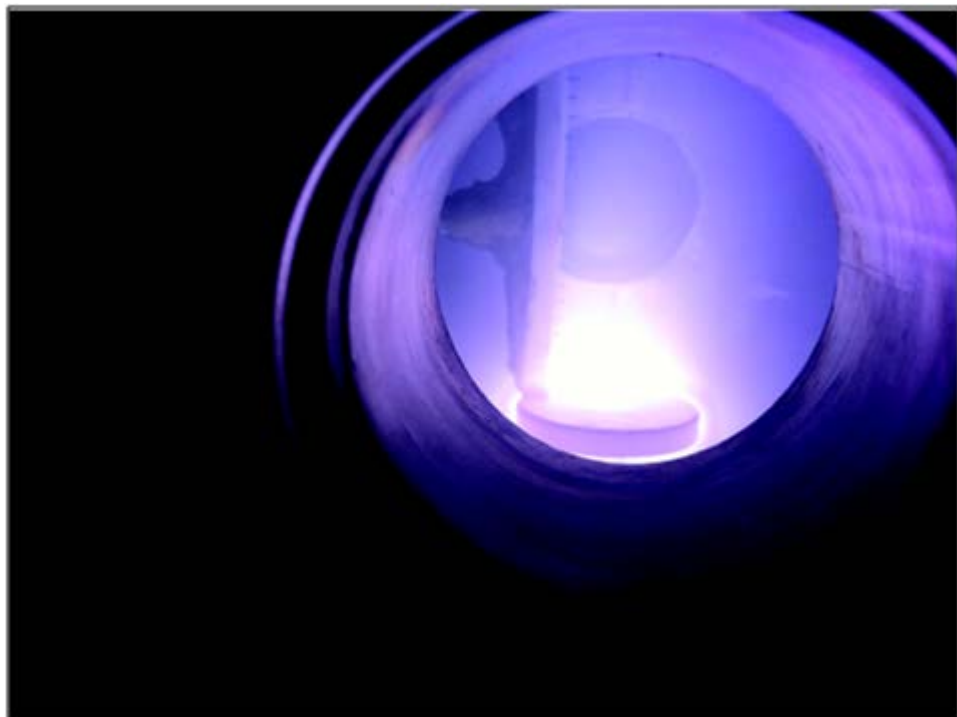


Figure 5.4. Probe measurements



Figure 5.5. The view of the glow discharge probe measurements at the outside of the chamber

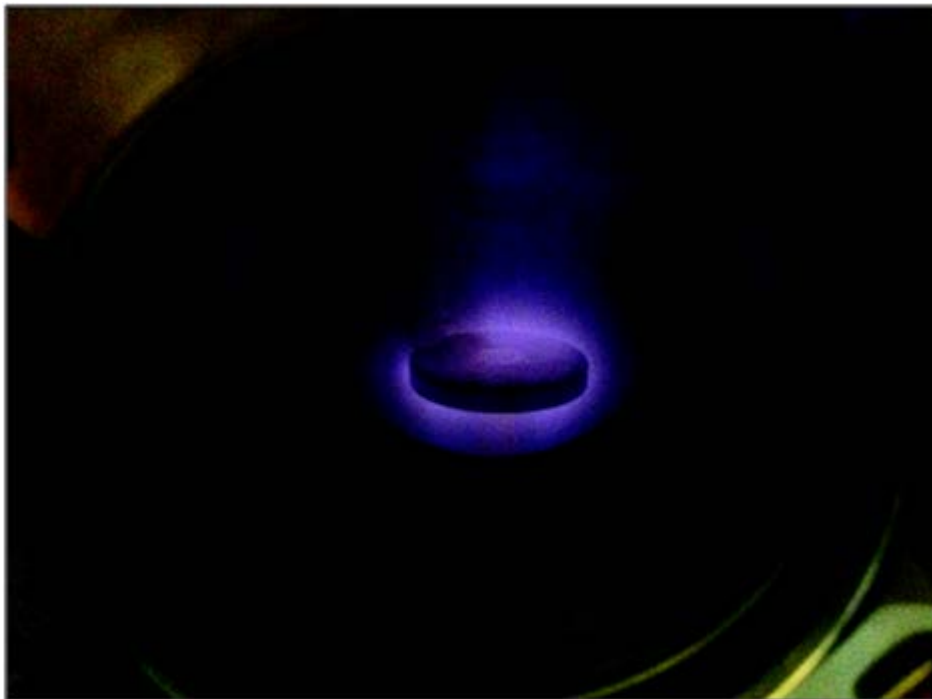


Figure 5.6. Glow discharge occurred around the cathode



Figure 5.7. Inside of the vacuum chamber with probes

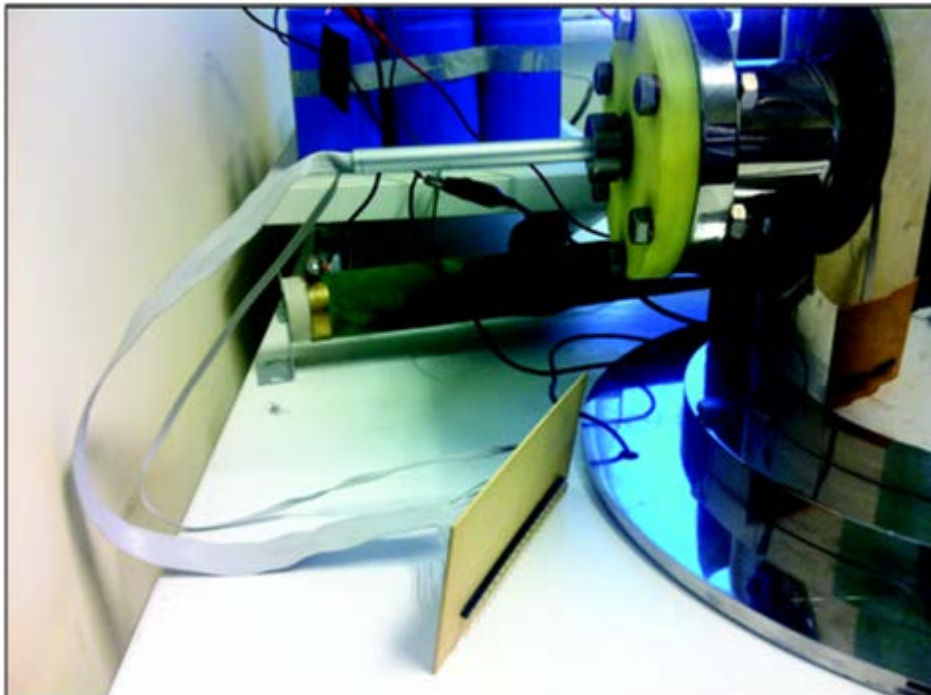


Figure 5.8. The measurements are taken between the subsequent 2 probes of 19

The first experiment conducted at the newly established laboratory has shown that there is an exponential proportionality between the pressure inside the chamber and time. When the vacuum system started to work, we have measured the pressure with respect to time. We have taken the values until the 30 *mTorr*. The graph has been sketched by using Stanford Graphics.

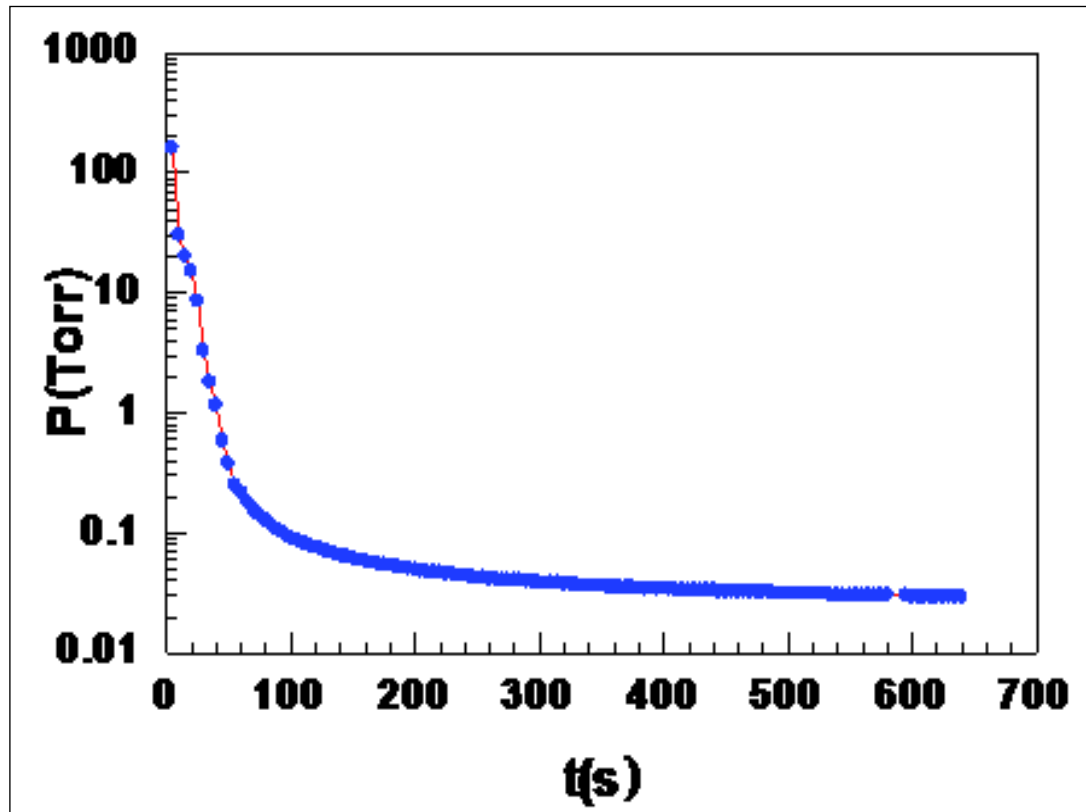


Figure 5.9. The change in pressure with time. The graphs have been sketched by using Stanford Graphics

5.1. BREAKDOWN VOLTAGE AND PASCHEN CURVES

Early vacuum experimenters found a rather surprising behaviour. An arc would sometimes take place in a long irregular path rather than at the minimum distance between the electrodes. Paschen [33] found that breakdown voltage was described by the equation

$$V = \frac{a(pd)}{\ln(pd)+b} \quad (5.1)$$

where V is the breakdown voltage in volts, p is the pressure, d is the gap distance. The constants a and b depend upon the composition of the gas. For air at standard atmospheric pressure of $101kPa$, $a = 43.6 V/(atm.m)$ and $b = 12.8$, where p is the pressure in atmospheres and d is the gap distance in meters. The graph of this equation is the Paschen curve. By differentiating it with respect to pd and setting the derivative to zero, the minimum voltage can be found. This yields

$$pd = e^{1-b} \quad (5.2)$$

and predicts the occurrence of a minimum breakdown voltage for $pd = 7.5 \times 10^{-6} m.atm$. This is $327 V$ in air at standard atmospheric pressure at a distance of $7.5 \mu m$. The composition of the gas determines both the minimum arc voltage and the distance at which it occurs. For argon, the minimum arc voltage is $137 V$ at a larger $12 \mu m$. With sulfur dioxide, the minimum arc voltage is $457 V$ at only $4.4 \mu m$. For air at *STP*, the voltage needed to arc a 1 meter gap is about $3.4 MV$. The intensity of the electric field for this gap is therefore $3.4 MV/m$. The electric field needed to arc across the minimum voltage gap is much greater than that necessary to arc a gap of 1 meter. For a $7.5 \mu m$ gap the arc voltage is $327 V$ which is $43 MV/m$. This is about 13 times greater than the field strength for the 1 meter gap. The phenomenon is well verified experimentally and is referred to as the Paschen minimum. The equation loses accuracy for gaps under about $10 \mu m$ in air at 1 atmosphere and incorrectly predicts an infinite arc voltage at a gap of about 2.7 micrometers.

In the experiments of Voltage V versus Pressure \times Separation distance (Pd), starting from $47 mTorr$ we have measured the voltage values until the $255 mTorr$ for air (mass flow meter was not enough to make higher measurements) and made similar measurements for argon from $33.5 mTorr$ to $185 mTorr$.

Table 5.1. The values of pressure \times separation distance and voltages for air

<i>Pd(mTcm)</i>	<i>V(volt)</i>
47	800
91	470
101	390
112	420
123	420
133	430
164	430
205	410
240	410
255	390

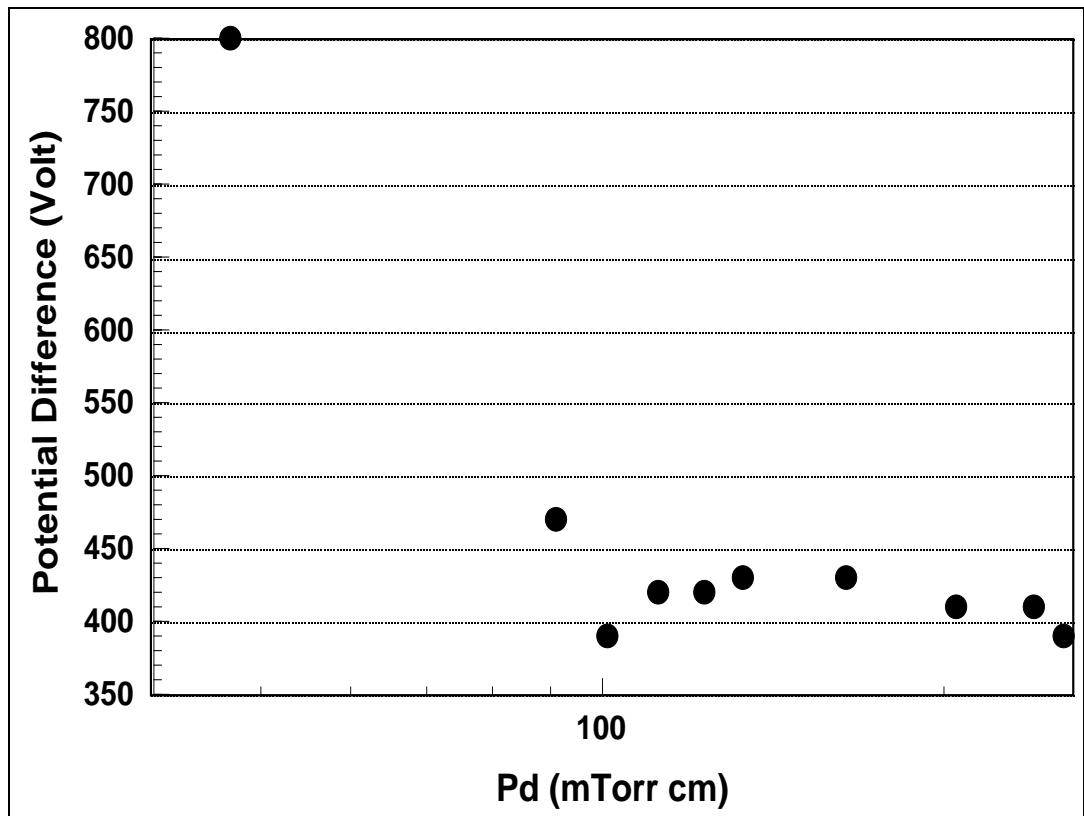


Figure 5.10. Voltage vs Pd for air. The graph have been sketched by using Stanford Graphics

Table 5.2. The values of pressure \times separation distance and voltages for Argon

$Pd(mT\ cm)$	$V(Volt)$
33.5	620
68.0	340
93.5	300
122	290
140	280
179	270
185	280

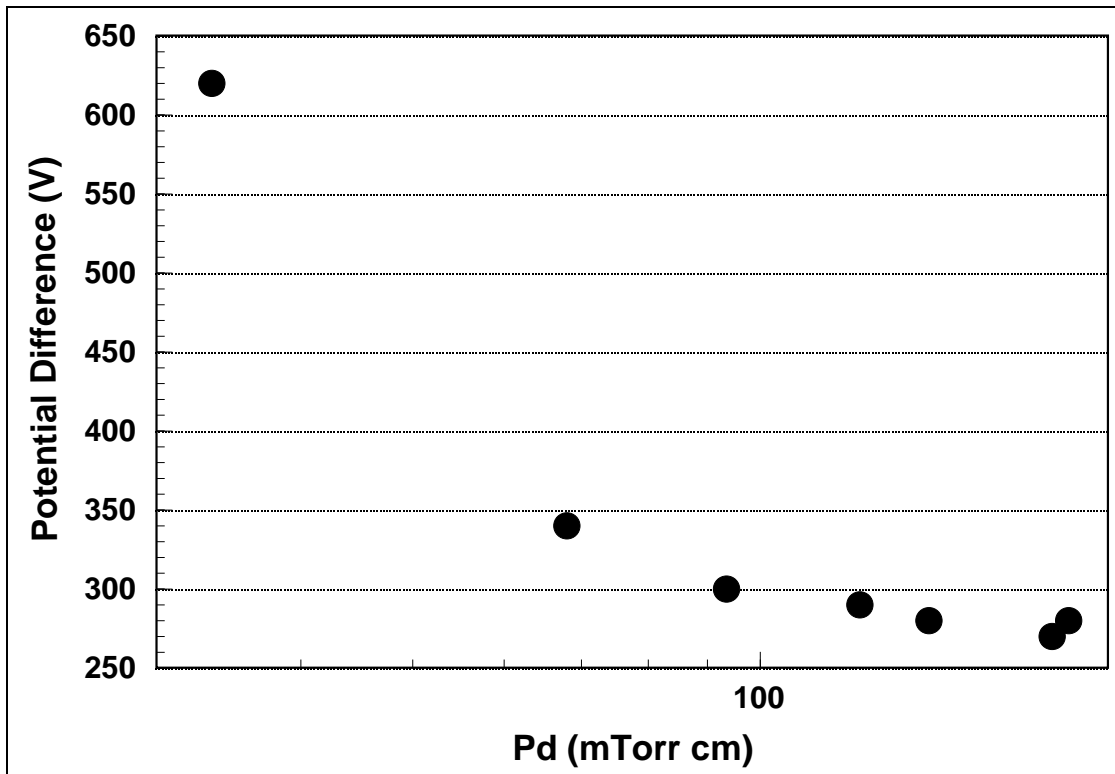


Figure 5.11. Voltage vs Pd for Argon. The graphs have been sketched by using Stanford Graphics

As it is seen from the graphs (or tables), argon reaches the breakdown voltage faster than air because air is difficult to ionize.

5.2. PROBE MEASUREMENTS

Table 5.3. Double probe measurements from the oscilloscope for air at the pressure of 40 and 60 *mTorr*

Probes	p=40 mT	p=60 mT
1	0.00	0.00
2	0.10	0.44
3	0.15	0.94
4	0.22	1.43
5	0.56	2.58
6	0.78	3.12
7	1.24	3.60
8	1.85	3.70
9	1.96	3.60
10	2.34	3.60
11	2.29	3.60
12	2.21	3.60
13	2.40	3.60
14	2.43	3.60
15	2.40	3.60
16	2.37	3.60
17	2.39	3.60
18	2.40	3.60
19	2.40	3.60

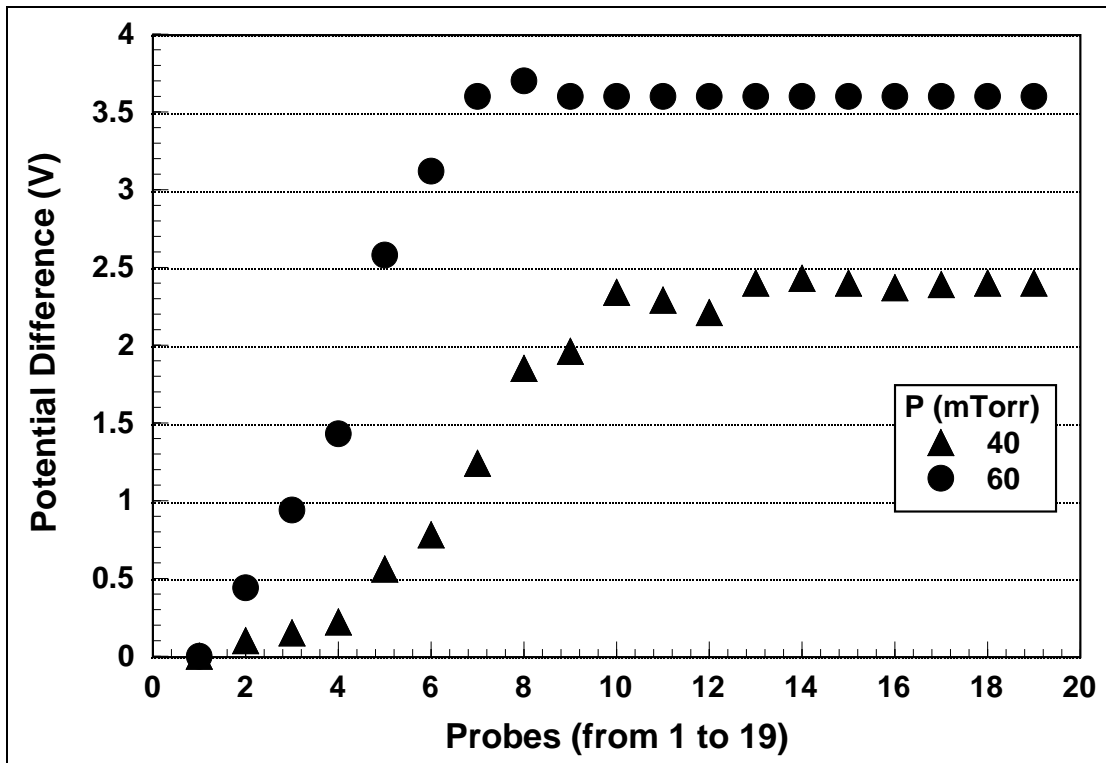


Figure 5.12. Double probe measurements from the oscilloscope for air at the pressure of 40 and 60 *mTorr*. The graphs have been sketched by using Stanford Graphics

It is evident that voltage is increased as the pressure increases and afterwards both remain constant. There is a good agreement with literature results.

Table 5.4. Double probe measurements from the multimeter for air at the pressure of
45.5 mTorr

Probe	P=45.5 mT
1	0.00
2	0.07
3	0.14
4	0.19
5	0.38
6	0.53
7	0.88
8	1.32
9	1.41
10	1.73
11	1.75
12	1.70
13	1.85
14	1.88
15	1.85
16	1.84
17	1.85
18	1.89
19	1.83

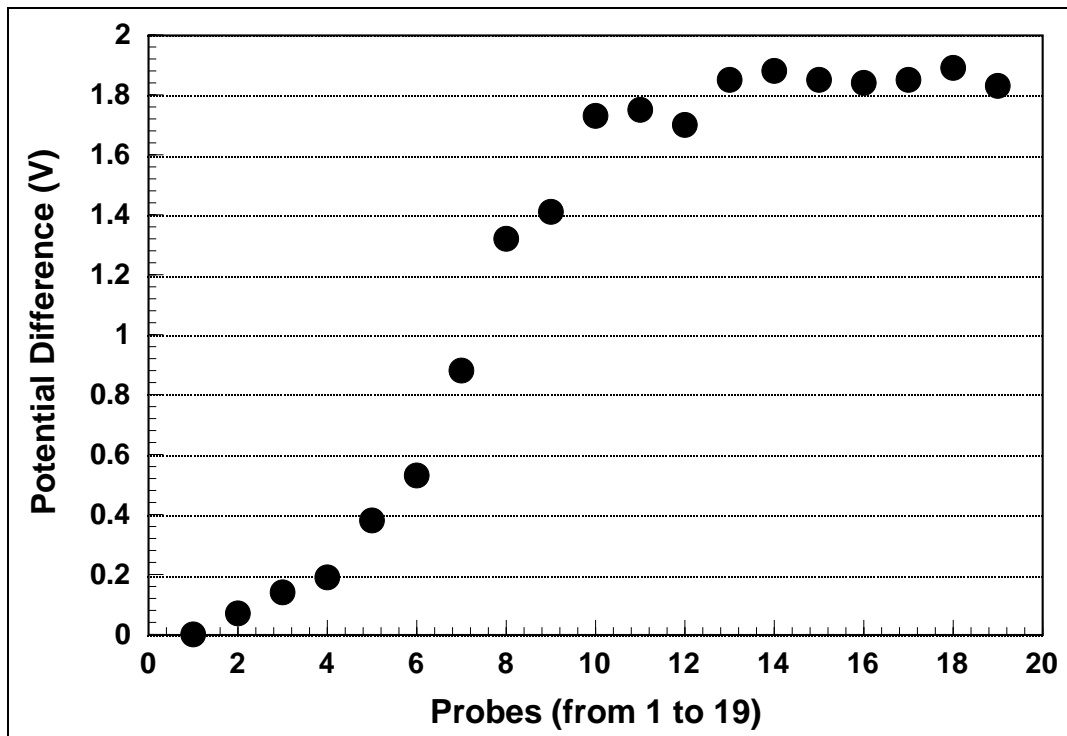


Figure 5.13. Double probe measurements from the multimeter for air at the pressure of 45.5 mTorr . The graphs have been sketched by using Stanford Graphics

In the second part of the probe measurements, a similar experiment was done with argon gas. Initially, there was a partially argon (approximately one quarter) at the pressure of 116 mTorr in the plasma. Again we have observed steady increase then reaching a constant value, which is consistent with the theory.

Table 5.5. Double probe measurements when there is partial ($\approx 1/4$)Ar at the pressure of 116 *mTorr*

Probes	P=116 mT
1	0.00
2	5.30
3	10.2
4	10.1
5	10.1
6	9.80
7	9.80
8	9.80
9	9.80
10	9.80
11	9.80
12	9.80
13	9.80
14	9.80
15	9.80
16	9.80
17	9.80
18	9.80
19	9.80

Next, we have increased the quantity of argon in the plasma, and then have taken the measurements at the pressures of 114 and 142 *mTorr* , respectively. The graph indicated that the voltage is increased with higher pressure.

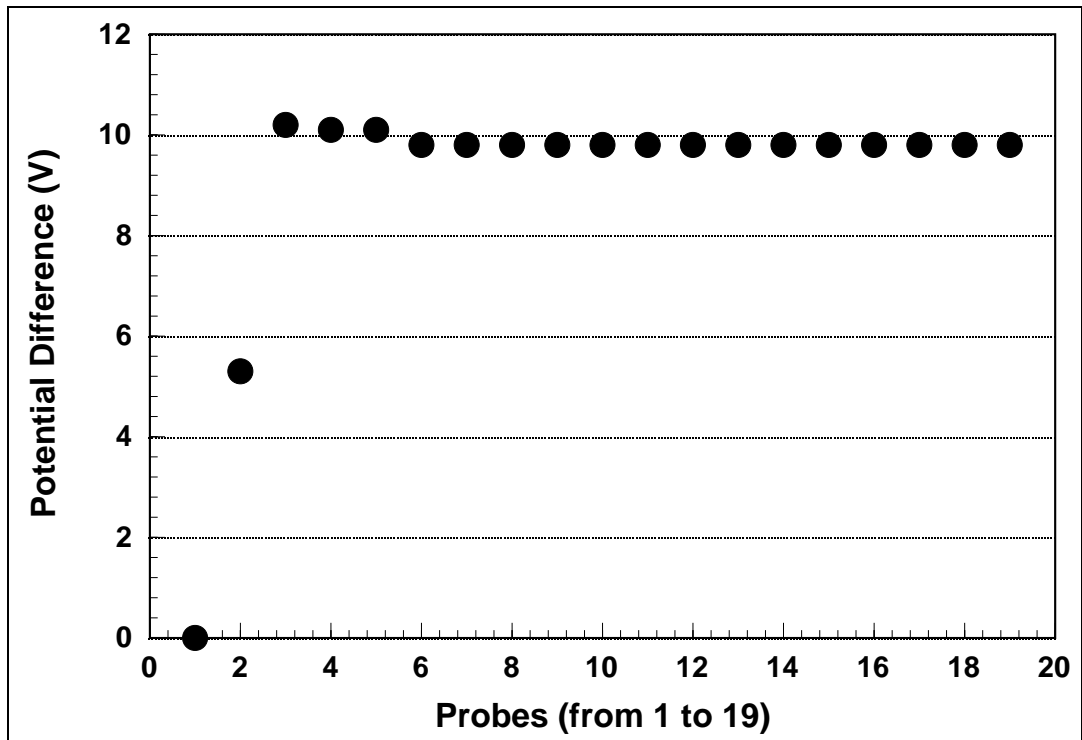


Figure 5.14. Double probe measurements when there is partial ($\approx 1/4$) Ar at the pressure of 116 *mTorr*. The graphs have been sketched by using Stanford Graphics

Table 5.6. Double probe measurements when there is mostly ($\approx 3/4$) Argon (Ar) at the pressure of 114 and 142 *mTorr*

Probes	p=114 mT	p=142 mT
1	0.00	0.00
2	1.70	0.68
3	1.98	0.92
4	1.60	0.62
5	1.35	0.91
6	1.10	0.42
7	1.62	1.00
8	1.58	0.71
9	2.10	1.38
10	2.30	1.40
11	2.28	1.25
12	2.35	1.27
13	2.90	1.80
14	3.20	2.10
15	3.00	1.70
16	3,00	1,70
17	3,12	1,70
18	3,20	1,70
19	3,25	1,70

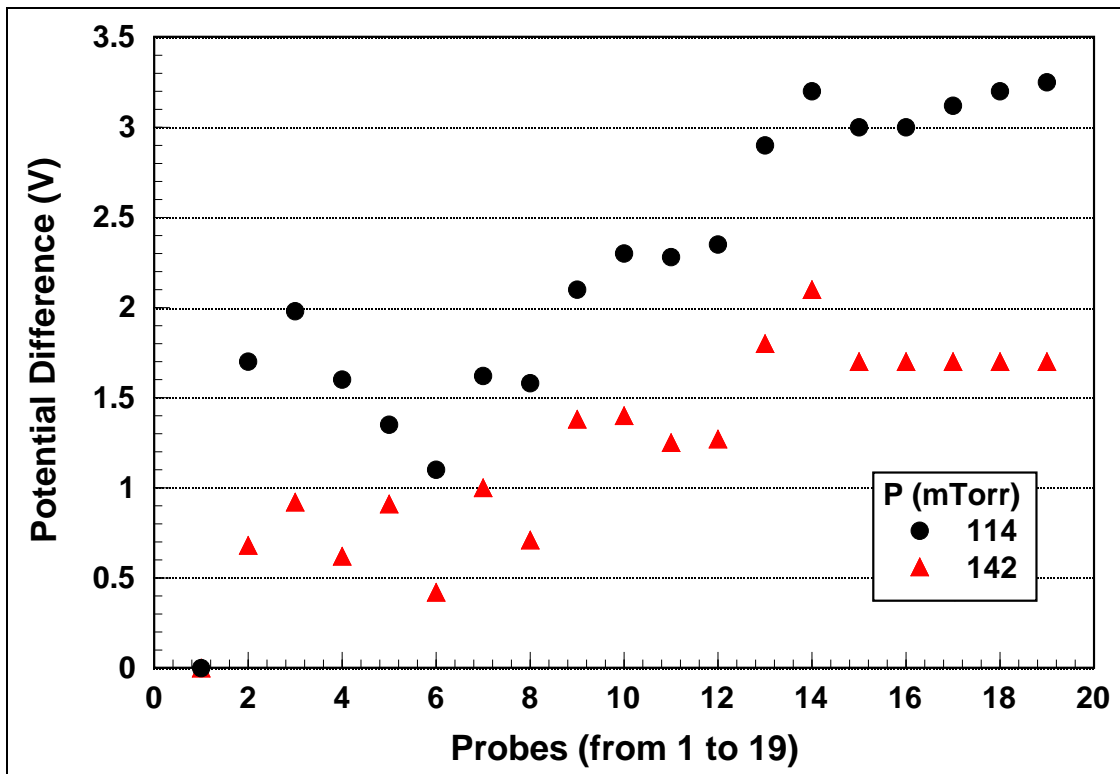


Figure 5.15. Double probe measurements when there is mostly ($\approx 3/4$) Argon (Ar) at the pressure of 114 and 142 *mTorr*. The graphs have been sketched by using Stanford Graphics

5.3 PLASMA DIAGNOSTICS

Finally, we have done some plasma diagnostics experiments. After creating the glow discharge plasma, using the BAKI spectrometer we have measured the wavelength and intensity of argon plasma at various pressures.

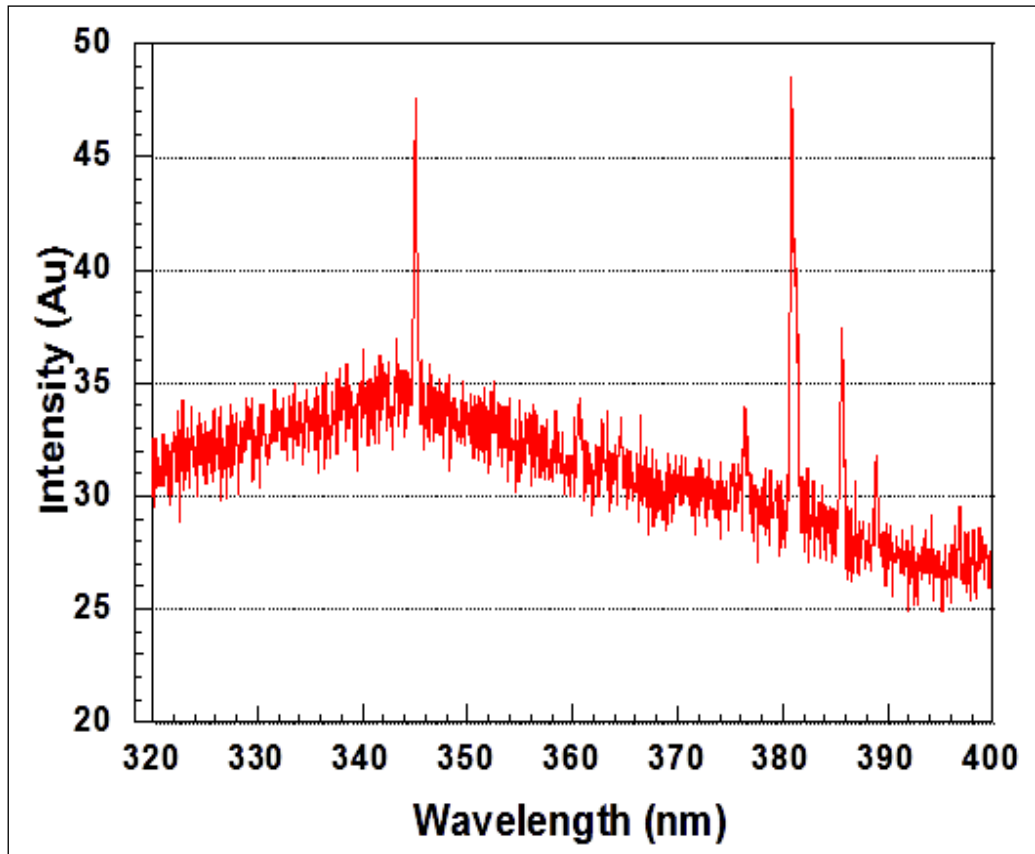


Figure 5.16. Background measurement of wavelength versus intensity at 30 *mTorr*. The graphs have been sketched by using Stanford Graphics

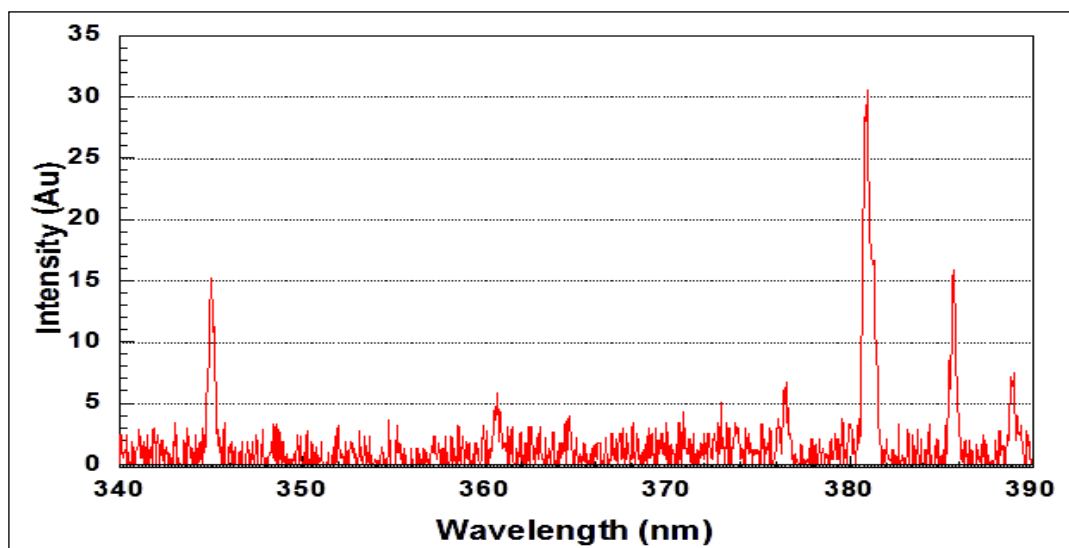


Figure 5.17. Wavelength versus intensity at high pressure of 90 *mTorr*. The graphs have been sketched by using Stanford Graphics

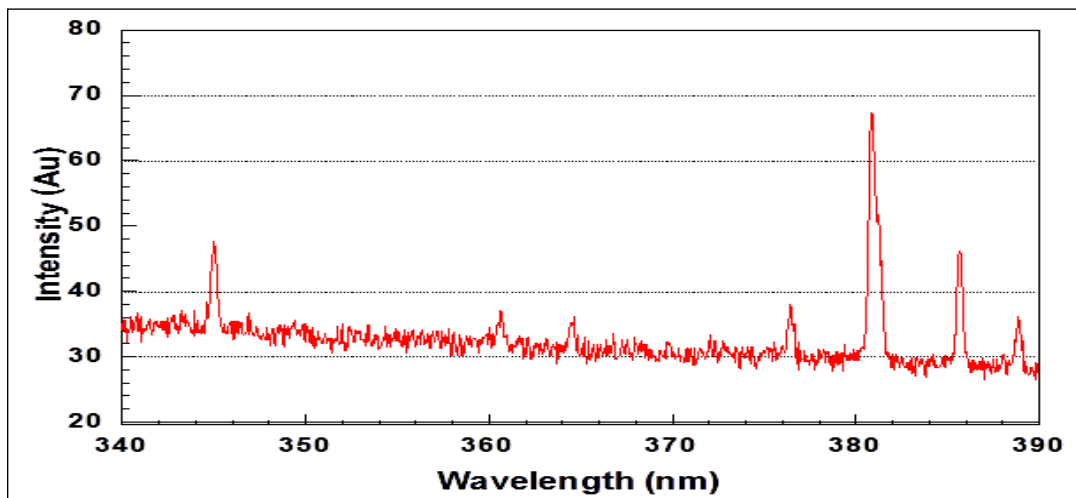


Figure 5.18. Background measurement of wavelength versus intensity at high pressure of 150 *mTorr*. The graphs have been sketched by using Stanford Graphics

At first, we have determined from the graph the wavelengths of the peaks having higher intensities. Then, using the NIST Atomic Spectra Database [34], we have found the generated ion species in Table 5.7. *O II* and *Ar II* has the same resolution.

Table 5.7. According to the locations of the peaks, the ions generated in the discharge

Ions	Wavelength (Å)
Ar II	3856.13749
O II	3856.13420
Fe I	3808.28140
N III	3450.40000

6. CONCLUSION

In this study, we have mainly covered the outcomes of the experiments conducted at the newly-established The Vacuum and Plasma Physics Laboratory of Yeditepe University. We have constructed a *DC* power supply. We can summarize our findings as follows:

1. There is an exponential relationship between pressure and time.
2. We have calculated breakdown voltage for air and argon.
3. We have made double probe measurements for air and argon.
 - We have observed that breakdown voltage is increased as the pressure increases.
 - There was a consistent increase in breakdown voltage and then it became steady as the literature suggests.
4. By using the emission spectroscopy, we have measured the wavelength and the intensity of argon plasma at various pressures.
5. Deciding the locations of the peaks, we have found the ions generated in the discharge.

The future work will include:

1. The similar experiments with N , H_2 and He ,
2. The investigations of $I - V$ characteristics of glow discharge plasma,
3. Langmuir probe measurements,
4. With higher sensitive equipments and *DC* power supply, more accurate results in further experiments.

7. REFERENCES

1. Chen, F. F., *Introduction to Plasma Physics and Controlled Fusion*, Volume 1, 2nd Edition, Plenum Press, New York, 1984.
2. Chapman, B.N., *Glow Discharge Processes*, Wiley and Sons, New York, 1980.
3. Fujimoto and Takashi, *Plasma Spectroscopy*, Clarendon Press, Oxford, 2004.
4. Franz, G., *Low Pressure Plasmas and Microstructuring Technology*, Springer-Verlag, Berlin Heidelberg, 2009.
5. Liebermann, M.A. and Lichtenberg A.C., *Principles of Plasma Discharges and Materials Processing*, Wiley, New York, 1994.
6. Nasser, E., *Fundamentals of Gaseous Ionization and Plasma Electronics*, Wiley Interscience, New York and London, 1971.
7. Cobine, J.D., *Gaseous Conductors*, Dover, New York, 1958.
8. Engel, A. von, *Ionized Gases*, Oxford University Press, 1965.
9. Rudberg, E., *Proc. Roy. Soc. (London)*, A127, 111 (1930).
10. Rudberg, E., *Physical Review*, 4, 764 (1934).
11. Hemenway C.L., Henry, R.W. and Caulton, M., *Physical Electronics*, Wiley and Sons, New York and London, 1967.
12. Hagstrum, H.D., *Physical Review*, 104, 672 (1956).
13. Hagstrum, H.D., *Physical Review*, 104, 1516 (1956).

14. Medved, D.B., Mahadevan, P., and Layton, J.K., *Physical Review*, 129, 2086 (1963).
15. Holmes, A.J.T., and Cozens, J.R., *J.Phys. D Appl. Phys.*, 7, 1723 (1974).
16. Davis, W.D., and Vanderslice, T.A., *Physical Review*, 131, 219 (1963).
17. Güntherschulze, A., *Z. Physik*, 59, 433 (1930).
18. Cruzan, P.D., and Tisone, T.C., *Journal of Vacuum Science and Technology*, 12, 1058, 1975.
19. Langmuir, I., "The Pressure Effect and Other Phenomena in Gaseous Discharges", *Journal of the Franklin Institute*, Vol. 196, Issue 6, pp. 751-762, 1923.
20. Langmuir, I. and Mott-Smith, H., *General Electric Review*, 26, 731(1923), 27, 449-538-616-762 and 810(1924).
21. Langmuir, I. and Mott-Smith, H., "The theory of collectors in gaseous electronics", *Physical Review* 28, 727-63, 1926.
22. Ball, D.J., *Journal of Applied Physics*, 43, 7, 3047 (1972).
23. Coburn, J.W. and Kay, E., *Journal of Applied Physics*, 43, 12, 4966 (1972).
24. Bohm, D., *The characteristics of Electrical Discharges in the Magnetic Fields*, ed. A.N. Guthrie and R.K. Wakerling, McGraw Hill, New York-London, 1949.
25. Chen, F. F., *Introduction to Plasma Physics*, Plenum Press, New York and London, 1974.
26. Chen, F.F., *Plasma Diagnostics Techniques*, ed Huddleston, R.H. and Leonard, S.L., Academic Press, 1965.

27. Laframboise, J.G., University of Toronto, *Institute of Aerospace Studies*, Report No:100, 1966.
28. Swift, J.D. and Schwar, M.J.R., *Electrical Probes for Plasma Diagnostics*, Iliffe, London, 1970.
29. Loeb, L.B., *Basic Processes of Gaseous Electronics*, University of California Press, Berkeley, 1961.
30. Clements, R.M., *Journal of Vacuum Science and Technology*, 15, 2, 193 (1978).
31. Thornton, *Journal of Vacuum Science and Technology*, 15, 2, 188 (1978).
32. Eser, E. Ogilvie, R.E. and Taylor, K. A., *Journal of Vacuum Science and Technology*, 15, 2, 199 (1978).
33. Paschen, F., *Wied. Ann.*, 37, 69, 1889.
34. Ralchenko, Yu., Kramida, A.E., Reader, J., and NIST ASD Team (2011). *NIST Atomic Spectra Database (ver. 4.1.0)*, [Online], <http://physics.nist.gov/asd> [2011, December 11]. National Institute of Standards and Technology, Gaithersburg, MD.